

NEW QUINOXALINE CONTAINING DONOR-ACCEPTOR TYPE CONJUGATED
POLYMERS FOR ORGANIC SOLAR CELLS

A THESIS SUBMITTED TO
THE GRADUATE SCHOOL OF NATURAL AND APPLIED SCIENCES
OF
MIDDLE EAST TECHNICAL UNIVERSITY

BY

ÖZGE KARAGAÇTI

IN PARTIAL FULFILMENT OF THE REQUIREMENTS
FOR
THE DEGREE OF MASTER OF SCIENCE
IN
CHEMISTRY

AUGUST 2018

Approval of the thesis:

**NEW QUINOXALINE CONTAINING DONOR-ACCEPTOR TYPE CONJUGATED
POLYMERS FOR ORGANIC SOLAR CELLS**

submitted by **ÖZGE KARAGAÇTI** in partial fulfillment of the requirements for the degree
of **Master of Science in Chemistry Department, Middle East Technical University** by,

Prof. Dr. Halil Kalıpçılar
Dean, Graduate School of **Natural and Applied Sciences**

Prof. Dr. Cihangir Tanyeli
Head of Department, **Department of Chemistry**

Prof. Dr. Ali Çırpan
Supervisor, **Department of Chemistry, METU**

Examining Committee Members:

Prof. Dr. Levent Toppare
Chemistry Dept., METU

Prof. Dr. Ali Çırpan
Chemistry Dept., METU

Prof. Dr. Yasemin Aslan Udum
Technical Sciences Vocational School, Gazi University

Assoc. Prof. Dr. Gülay Ertaş
Chemistry Dept., METU

Assoc. Prof. Dr. Görkem Günbaş
Chemistry Dept., METU

Date: 07/08/2018

I hereby declare that all information in this document has been obtained and presented in accordance with academic rules and ethical conduct. I also declare that, as required by these rules and conduct, I have fully cited and referenced all material and results that are not original to this work.

Name, Last name: Özge Karagaçtı

Signature:

ABSTRACT

NEW QUINOXALINE CONTAINING DONOR-ACCEPTOR TYPE CONJUGATED POLYMERS FOR ORGANIC SOLAR CELLS

Karagaçtı, Özge

M.S., Department of Chemistry

Supervisor: Prof. Dr. Ali Çırpan

August 2018, 87 pages

In this study, quinoxaline, benzotriazole and benzodithiophene containing three random donor-acceptor type copolymers were synthesized and their electrochemical, spectroelectrochemical, kinetic and photovoltaic properties were investigated. Quinoxaline demonstrates electron accepting properties due to having imine nitrogens. Also, benzotriazole derivatives with their electron withdrawing imine groups in their structures also lead to exhibit high electron transporting ability. Benzodithiophene derivatives demonstrate electron donor property because the structure of benzene with coherent thiophene gives these polymers high hole mobility. In addition, alkoxy groups in benzodithiophene derivatives help to increase the solubility of the polymer. Bringing together these three groups yields the conjugated copolymer with broad absorption band in the visible region. This study includes the construction of random copolymers by using quinoxaline derivatives (5,8-dibromo-2,3-di(thiophen-2-yl) quinoxaline, 5,8-dibromo-2,3-diphenylquinoxaline, 10,13-dibromo-8b,14a-dihydrodibenzo(a,c)phenazine) and 2,6-Bis(trimethylstannyl)-4,8-bis(2-ethylhexyloxy)benzo[1,2-b:4,5-b']dithiophene and 4,7-dibromo-2-(2-octyldodecyl)-2H-benzo[d][1,2,3]triazole. ¹H and ¹³C-NMR Spectroscopy were used to investigate the structure of monomers and polymers. Produced polymers were utilized as donor material and PC₇₁BM was used as

acceptor material in bulk hetero-junction photovoltaic devices. Power conversion efficiencies of solar cell devices with different Polymer: PC₇₁BM ratios (w:w) were measured under AM 1.5 G illumination (100 mW/cm²) and best PCE value was recorded as 2.22 % with 1:4 (w:w) P2: PC₇₁BM blend ratio.

Keywords: benzodithiophene, benzotriazole, conjugated polymers, quinoxaline, organic solar cells, random copolymers, Stille coupling reaction

ÖZ

ORGANİK GÜNEŞ PİLLERİ İÇİN YENİ KİNOKSALİN İÇERİKLİ DONÖR- AKSEPTÖR TİPİ KONJUGE POLİMERLER

Karagaçtı, Özge
Yüksek Lisans, Kimya Bölümü
Tez Yöneticisi: Prof. Dr. Ali Çırpan
Ağustos 2018, 87 sayfa

Bu çalışmada, kinoksalin, benzotriazol ve benzodityofen içeren üç adet rastgele polimer sentezi yapılmış olup, bu polimerlerin elektrokimyasal, spektroeletrokimyasal, kinetik ve fotovoltaiik özellikleri incelenmiştir. İmin grubuna sahip olmasından dolayı kinoksalin, elektron akseptör özelliği göstermektedir. Aynı şekilde yapılarında bulunan imin gruplarının elektron çekici özelliği ile benzotriazol türevleri de yüksek elektron taşıma yeteneğine sahiptirler. Benzodityofen temelli kopolimerler benzen halkasına yapışık tiyofenlerden oluşan yapısından kaynaklanan yüksek boşluk mobilitesi sayesinde donör özelliği gösterirler. Buna ek olarak, benzodityofen türevlerindeki alkoksil grupları polimerin çözünürlüğünü arttırmaya yardımcı olmaktadır. Bu üç grubun biraraya gelmesiyle konjuge polimerler, görünür bölgede geniş bir soğurmaya sahip olur. Bu çalışma, 5,8-dibromo-2,3-di(tiyofen-2-il)kinoksalin, 5,8-dibromo-2,3-difenilkinoksalin, 10,13-dibromo-8b,14a-dihidrobenzo(a,c)fenazin gibi kinoksalin türevleri ile 2,6-Bis(trimetilstanil)-4,8-bis(2-etilheksiloksi)benzo[1,2-b:4,5-b']dityofen ve 4,7-dibromo-2-(2-oktildodesil)-2H-benzo[d][1,2,3]triazol kullanarak rastgele polimerlerin elde edilmesini kapsamaktadır.¹H ve ¹³C NMR Spetrokopisi monomer ve polimer yapılarını tayin etmek amacıyla kullanılmıştır. Üretilen polimerler yığın heterobağlantılı güneş pillerinde donör materyalleri olarak kullanılırken, PC₇₁BM akseptör olarak kullanılmıştır. Farklı ağırlıklı oranlarda hazırlanan polimer PC₇₁BM karışımları ile

elde edilen güneş pillerinin verimleri AM 1.5G aydınlatması ile (100 mW/cm^2) ölçülmüştür. En iyi güneş pili verimi değeri 1:3 Polimer: PC₇₁BM karışımıyla P2 polimeri için % 2.22 olarak kaydedilmiştir.

Anahtar Kelimeler: benzodityofen benzotriazol, konjüge polimerler, kinoksalin, organik güneş pilleri, rastgele polimerler, Stille kenetleme reaksiyonu.

To my lovely family

ACKNOWLEDGEMENTS

First of all, I would like to express my profound gratitude to my supervisor Prof. Dr. Ali Çırpan for his collaboration, guidance, patience, support and optimistic attitude throughout my master study.

I would also like to offer my special thanks for Prof. Dr. Levent Toppare for his scientific expertise and contributions with his valuable comments on this thesis.

I am grateful to Dr. Şerife Hacıoğlu and Dr. Gönül Hızalan for providing guidance and exertions on electrochemical and photovoltaic studies and also to Şevki Can Cevher for his precious guidance and support during synthesis period of this thesis.

I would like to express my feelings to Aslı Çetin for being the best laboratory partner for all experiments, courses, assignments and hard tasks and for being a shoulder to cry on during my thesis.

I owe a dept of gratitude especially for three special people, Soner, Özge and Duygu and also my all lab mates İpek, Ece, Janset, Kardelen, Merve, Emre, Sultan, Duygu, and Dr. Fatma Demir for their friendships and providing such a good working environment.

I would like to thank my precious friends Büşra Köşki, Asena Çerçi, Betül Karantinalı, Hazan Altuğ, Merve Çetin, Nihal Karaman and Özge Turan for their friendships.

Special thanks to Duygu Yaslak for her sensible and wise advices and encouragements. She was one of my best supporters not only during my thesis study but also during my whole university years.

I would like to offer my deepest thanks to Onur Dursun for supporting me through the hardest times with his endless love and understanding. He was always there when I need him. He is the best supporter in my life.

The last but not the least, I owe a lot to my precious father and mother for their endless love, guidance and encouragement. My thesis journey would not have been without their powerful support of them, I would like to also thank to my sister and life advisor Gamze Akagündüz and my brother in law Görkem Akagündüz for their help and support during my thesis study.

TABLE OF CONTENTS

ABSTRACT	v
ÖZ.....	vii
ACKNOWLEDGEMENTS	x
TABLE OF CONTENTS	xii
LIST OF TABLES	xvi
LIST OF FIGURES.....	xvii
ABBREVIATIONS	xix
CHAPTERS	
1. INTRODUCTION.....	1
1.1. Conjugated Polymers.....	1
1.2. Band Theory	2
1.3. Doping Process	4
1.4. Band Gap Engineering.....	6
1.4.1. Bond Length Alternation.....	7
1.4.2. Aromaticity.....	7
1.4.3. Planarity	8
1.4.4. Substituent Effects.....	8
1.4.5. Intermolecular Interactions.....	8
1.5. Donor-Acceptor Approach	9
1.6. Synthesis Methods for Conjugated Polymers.....	10
1.7. Moieties in Donor-Acceptor Approach Conjugated Polymers.....	13
1.8. Applications of Conducting Polymers.....	15

1.9. Electrochromism.....	15
1.9.1 Parameters Affecting Electrochromic Devices	18
1.9.1.1. Optical Contrast	18
1.9.1.2. Coloration Efficiency.....	18
1.9.1.3. Switching Time.....	19
1.9.1.4. Optical Memory	19
1.9.1.5. Stability.....	19
1.10. Organic Solar Cells.....	20
1.10.1. Device Architecture of Organic Solar Cells.....	20
1.10.1.1. Bilayer Solar Cells.....	20
1.10.1.2. Tandem Solar Cells	21
1.10.1.2. Bulk Heterojunction Organic Solar Cells.....	22
1.10.2. Mechanism of Organic Solar Cells	23
1.10.3. Characterization of a Solar Cell Device.....	25
1.10.4. Basic Factors Affecting Efficiency of an Organic Solar Cell	26
1.10.4.1. Open Circuit Voltage	26
1.10.4.2. Short Circuit Current.....	27
1.10.4.3. Fill Factor	28
1.11. Quinoxaline Containing Polymer Solar Cells.....	29
1.12. Aim of the Study.....	31
2. EXPERIMENTAL	35
2.1 Materials and Equipments	35
2.2. Synthesis of Monomers	36
2.2.1. Synthesis of 9-(bromomethyl)nonadecane.....	36
2.2.2. Synthesis of 4,7-dibromobenzo[c][1,2,5]thiadiazole.....	37

2.2.3.	Synthesis of 3,6-dibromobenzene-1,2-diamine.....	37
2.2.4.	Synthesis of 4,7-dibromo-2H-benzo[d][1,2,3]triazole.....	38
2.2.5.	Synthesis of 4,7-dibromo-2-(2-octyldodecyl)-2H-benzo[d][1,2,3]triazole.....	39
2.2.6.	Synthesis of 5,8-dibromo-2,3-di(thiophen-2-yl)quinoxaline	40
2.2.8.	Synthesis of 10,13-dibromodibenzo[a,c]phenazine	41
2.3.	Synthesis of Polymers	42
2.3.1.	Synthesis of P1	42
2.3.2.	Synthesis of P2	43
2.3.3.	Synthesis of P3	44
2.4.	Characterization of Conducting Polymers.....	45
2.4.1.	Gel Permeation Chromatography.....	45
2.4.2.	Electrochemical Studies.....	45
2.4.3.	Spectroelectrochemical Studies	46
2.4.4.	Kinetic Studies	46
2.4.5.	Thermal Studies	47
2.4.6.	Photovoltaic Studies.....	47
3.	RESULTS AND DISCUSSION	49
3.1.	Optical Studies.....	49
3.2.	Electrochemical Studies.....	51
3.3.	Spectroelectrochemical Studies	54
3.4.	Kinetic Studies.....	59
3.5.	Thermal Studies.....	61
3.6.	Photovoltaic Studies	61
3.7.	Morphology	67

4. CONCLUSIONS.....	69
REFERENCES.....	71
APPENDICES.....	81
A. NMR DATA.....	81
B. THERMAL ANALYSES RESULTS.....	85

LIST OF TABLES

TABLES

Table 1. Summary of the optical studies of P1, P2 and P3 in chloroform solution and thin film form	49
Table 2. Electrochemical Properties of P1, P2 and P3	54
Table 3. Spectroelectrochemical results of P1, P2 and P3	55
Table 4. L,a,b values of P1, P2 and P3.....	57
Table 5. Optical contrast and switching time values of P1, P2 and P3	59
Table 6. Summary of the photovoltaic studies of P1	65
Table 7. Summary of the photovoltaic studies of P2	65
Table 8. Summary of the photovoltaic studies of P3	66

LIST OF FIGURES

FIGURES

Figure 1. Repeating unit structures of widely used conjugated polymers	2
Figure 2. Band Gap Structures of Metals, Semiconductors and Insulators	4
Figure 3. Scheme of p and n-type doping processes of organic semiconductors	5
Figure 4. Parameters affecting band gap of aromatic linear π -conjugated systems.....	7
Figure 5. Formation of new HOMO-LUMO energy levels and band gap.....	10
Figure 6. Proposed electrochemical polymerization mechanism of thiophene.....	11
Figure 7. Synthetic mechanism of palladium catalyzed cross coupling reactions.....	13
Figure 8. Oxidation-reduction process of viologens	17
Figure 9. Bilayer heterojunction solar cell device structure	21
Figure 10. Tandem solar cell device structure	22
Figure 11. Device architecture of bulk heterojunction solar cell.....	23
Figure 12. Working principle of organic solar cell	24
Figure 13. Current density-voltage characteristics of OSC under dark and illumination	26
Figure 14. Structures of H1, P(BDT-Qx), PBDT-DBPx and PBDTThQx	30
Figure 15. Structure of CoP1, CoP2 and CoP3	31
Figure 16. Structure of synthesized copolymers P1, P2 and P3.....	33
Figure 17. Synthesis of 9-(bromomethyl)nonadecane	36
Figure 18. Synthesis of 4,7-dibromobenzo[c][1,2,5]thiadiazole.....	37
Figure 19. Synthesis of 3,6-dibromobenzene-1,2-diamine	37
Figure 20. Synthesis of 4,7-dibromo-2H-benzo[d][1,2,3]triazole	38
Figure 21. Synthesis of 4,7-dibromo-2-(2-octyldodecyl)-2H-benzo[d][1,2,3]triazole	39
Figure 22. Synthesis of 5,8-dibromo-2,3-di(thiophen-2-yl)quinoxaline.....	40
Figure 23. Synthesis of 5,8-dibromo-2,3-diphenylquinoxaline	40
Figure 24. Synthesis of 10,13-dibromodibenzo[a,c]phenazine.....	41
Figure 25. Synthesis of P1	42

Figure 26. Synthesis of P2.....	43
Figure 27. Synthesis of P3.....	44
Figure 28. Absorption spectra of P1, P2 and P3 in chloroform solution and thin film form	50
Figure 29. Single-scan cyclic voltammograms of polymer films in 0.1 M TBAPF ₆ /ACN electrolyte solution a) P1 b) P2 c) P3.....	52
Figure 30. UV-Vis-NIR spectra and colors at different potentials of a) P1 , b) P2 and c) P3 in 0.1 M TBAPF ₆ /ACN electrolyte solution.....	58
Figure 31. Percent transmittance change of a) P1 b) P2 c) P3 in 0.1 M TBAPF ₆ / ACN electrolyte solution at given wavelengths	60
Figure 32. Energy levels of materials utilized in organic solar cell device construction	61
Figure 33. Current density-voltage curve of devices with P1	63
Figure 34. Current density-voltage curve of devices with P2	63
Figure 35. Current density-voltage curve of devices with P3	64
Figure 36. IPCE curves of best performance solar cells of P1, P2 and P3	66
Figure 37. AFM and TEM Images of a) P1:PC71BM (1:3) and b) P2:PC71BM (1:4) and a) P1:PC71BM (1:2).....	68
Figure 38. ¹ H NMR result of 4,7-dibromo-2-(2-octyldodecyl)-2H-benzo[d][1,2,3]triazole	81
Figure 39. ¹ H NMR result of 5,8-dibromo-2,3-di(thiophen-2-yl)quinoxaline.....	82
Figure 40. ¹ H NMR result of 5,8-dibromo-2,3-diphenylquinoxaline.....	82
Figure 41. ¹ H NMR result of 10,13-dibromodibenzo[a,c]phenazine.....	83
Figure 42. ¹ H NMR result of P1	83
Figure 43. ¹ H NMR result of P1	84
Figure 44. ¹ H NMR result of P3.....	84
Figure 45.TGA result of P1	85
Figure 46. TGA result of P2.....	85
Figure 47.TGA result of P3	86
Figure 48. DSC result of P1	86
Figure 49. DSC result of P2	87
Figure 50. DSC result of P3	87

ABBREVIATIONS

HOMO	Highest Occupied Molecular Orbital
LUMO	Lowest Unoccupied Molecular Orbital
VB	Valence Band
CB	Conduction Band
BLA	Bond Length Alternation
REPE	Resonance Energy per Electron
D	Donor
A	Acceptor
EC	Electrochromic
OLED	Organic Light Emitting Diode
L_D	Exciton Diffusion Length
OFET	Organic Field Effect Transistor
OPV	Organic Photovoltaics
BTz	Benzo[d][1,2,3]triazole
BDT	Benzo[1,2-b:4,5-b']dithiophene
PEDOT	Poly(3,4-ethylenedioxythiophene)
PSS	Polystyrene sulfonate
PCBM	[6,6]-Phenyl-C ₆₁ -butyric acid methyl ester
MPP	Maximum Power Point
PCE	Power Conversion Efficiency
ITO	Indium Tin Oxide
PDI	Polydispersity Index
GPC	Gel Permeation Chromatography
CV	Cyclic Voltammetry
WE	Working Electrode
CE	Counter Electrode
RE	Reference Electrode

TBAPF₆	Tetrabutylammoniumhexafluorophosphate
ACN	Acetonitrile
UV	Ultraviolet
Vis	Visible
IR	Infrared
<i>V_{oc}</i>	Open Circuit Voltage
<i>I_{sc}</i>	Short Circuit Current
<i>J_{sc}</i>	Short Circuit Current Density
FF	Fill Factor
<i>P_{in}</i>	Incident Light Power Density
THF	Tetrahydrofuran
DCM	Dichloromethane
E_g^{op}	Optical Band Gap
E_g^{el}	Electronic Band Gap

CHAPTER 1

INTRODUCTION

1.1. Conjugated Polymers

Until three decades ago, well known polymers were regarded as good insulators and placed in insulating device applications both in industry and academia. The phenomenon of conjugated polymers has been suggested at the beginning of 1977 in University of Pennsylvania by Shirakawa and his co-workers. They published an accidental study which states that conductivity of thin film state of polyacetylene increases significantly by doping processes with limiting amount of halogens. They reported the formation of new silver film form instead of expected black solid which showed altered optical properties as compared to the previous product. This discovery was enhanced with additional researches conducted by various other researches. Later on, Alan J. Heeger, Alan G. MacDiarmid and Hideki Shirakawa deemed to deserve the Nobel Prize in 2000.¹

Conducting polymers are organic macromolecules that have the ability of conducting electricity thanks to their extended π -orbital systems along which electrons can freely travel.² The most widely used examples of conjugated polymers are polyacetylene, polypyrrole, polythiophene, polyaniline, polyfuran, polythiophene and polyphenylene vinylenes. Their repeating units were shown in Fig. 1. These materials have been gained great attention because of their absorption ability and ease of deposition on flexible surfaces.³ CPs were utilized in many technological applications including Organic Light Emitting Diodes (OLEDs), Organic Solar Cells (OSCs), Biosensors and Electrochromic Devices (ECDs).^{4,5,6,7}

Electrical conductivity of a conjugated polymer can be supplied by fulfilling two basic requirements. The first one is possession of an orbital system that allows the movement of charge carriers along the polymer backbone. The second one is presence of the charge carriers. Conjugated polymers implement the former thanks to continuous overlapping of π -orbitals throughout the polymer chain. The latter can be provided by the application of doping processes.⁸

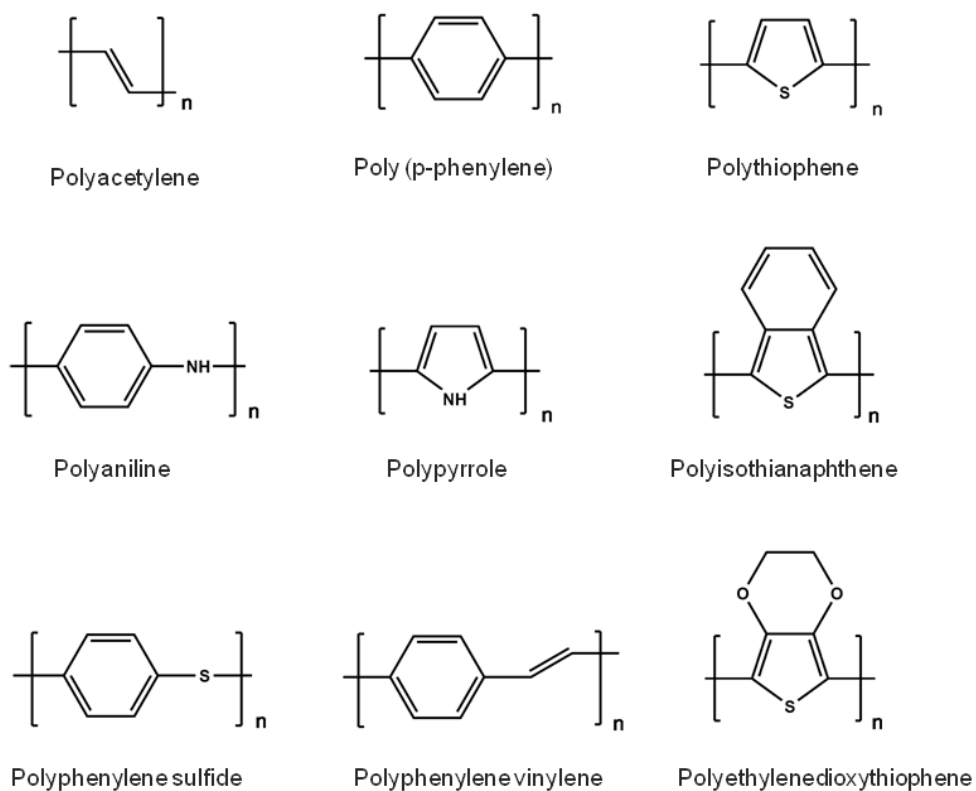


Figure 1. Repeating unit structures of widely used conjugated polymers

1.2. Band Theory

Band theory includes the classification of solid materials with respect to their ability to conduct electricity. According to the theory, electrical conductivity of a material is

related with the differences between highest occupied molecular orbital (HOMO) and lowest unoccupied molecular orbital (LUMO) of the material, which is known as band gap (E_g). For polymeric materials, HOMO is described as valance band (VB) and LUMO is called as conduction band (CB).⁹ Conductivity of a material can be achieved by migration of electrons from VB to CB.

According to their conduction ability, solid materials are divided into three groups including conductors, semiconductors and insulators. Band gap structures of three types of materials are shown in Figure 2. Conductors or metals have adjunctive CB and VB structure like a single band due to overlapping. In a conductive system, only incomplete energy levels could contribute to the transportation of charges.¹⁰ The valance band of a metal is partially filled and electrons can freely travel to empty positions with applied electric field. Then, conduction of electricity can be achieved. On the other hand, due to the large energy difference between valance and conduction bands, insulators have entirely full VB and quite empty CB. This arrangement prevents the movement of electrons therefore insulators could not conduct electricity. Many of the conventional polymers demonstrate fully filled VB and empty CB with a huge space between them.

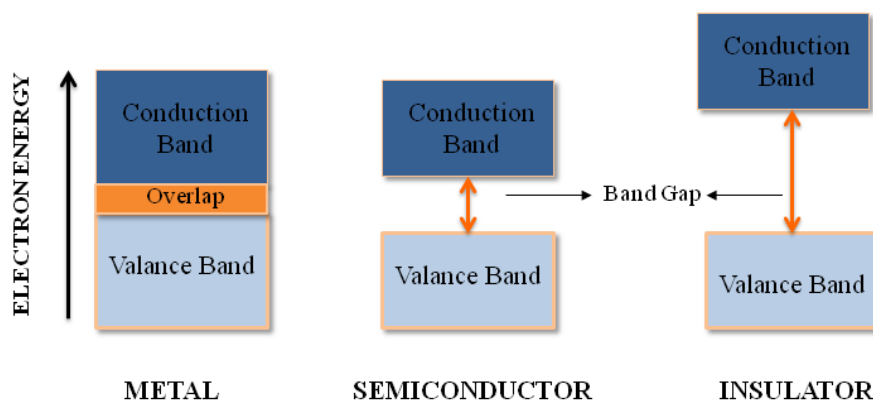


Figure 2. Band Gap Structures of Metals, Semiconductors and Insulators

Semiconductors take place between conductors and insulators in this classification. They neither have low band gap as metals nor high band gap like insulators. They demonstrate partially filled VB and empty CB resulting with freedom of action for excited electrons to conduct electricity. Thanks to their π conjugated structures and alternating single-double bonds, conductive polymers allow the transportation of electrons from the beginning of chain to the end.¹¹ Therefore, they are regarded as semiconductors according to band theory. For conjugated polymers, π -band is accepted as VB and π^* band is regarded as CB. Band gap of a conjugated polymer plays important role on its optical and electronic properties. Therefore, band gap engineering is assigned to control and arrange band gap of the materials.

1.3. Doping Process

As mentioned in Section 1.1. since conjugated polymers could not contain essential charge carriers along their backbones, charge carriers are provided either by partial oxidation called “p-doping” (anionic doping) or partial reduction known as “n-doping” (cationic doping) processes. P-type doping mechanism involves removal of electrons from the valance band of the polymer by oxidizing agent. Also, donation of

the electrons from reducing agent to the conduction band of the polymer generates the n-type doping. While p-type doping can be achieved by electron acceptors including Br_2 , I_2 or AsF_5 , electron donors such as Na, Li or K are utilized for n-type doping mechanism.

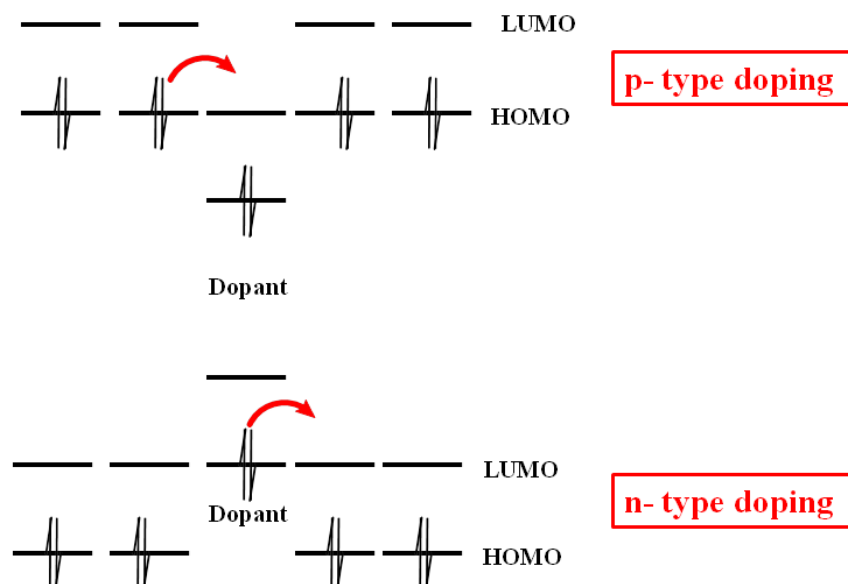


Figure 3. Scheme of p and n-type doping processes of organic semiconductors

During both procedures, electron transportation between polymer and oxidizing/reducing agents causes formation of partially filled valance/conduction bands and thus, radical anion/cation chains called as polarons. Also, removing or adding another electron to polymer backbone results in the formation of dianions/dications named as bipolarons. For non-degenerated ground state molecules, polarons and bipolarons are produced while for the degenerate ground state materials such as polyacetylene solitons are formed by redox reactions. Formed polarons, bipolarons or solitons could overlap which results in the formation of a transition band between CB and VB. This new transition band allows the electron flow and conductivity can be achieved in this way.^{8,12}

Doping mechanism plays a fundamental role in electrical properties of the conjugated polymers. Selection of the proper technique is a critical issue to obtain high conductivity after doping process. Application of these important processes to a conductive polymer can be made by five main techniques including electrochemical, chemical, in-situ, photo and charge-injection doping. Electrochemical and chemical techniques are the most commonly used ones. While electrochemical doping setup is consist of the standard three-electrode system including a working electrode, counter electrode and reference electrode, chemical doping mechanism contains the exposure of conducting polymer to vapour of an oxidative or reductive dopant.¹³

1.4. Band Gap Engineering

Electronic and optical characteristics of a conjugated polymer are identified by its band gap and band gap of a semiconductor depends on different parameters. Band gap engineering includes development and implementation of different strategies to tune and modify band gap of a conductive polymer. Band gap is calculated by contribution of a number of parameters with the following formula;

$$E_g = E_{Bla} + E_{Res} + E_{\theta} + E_{Sub} + E_{int}$$

Where E_{Bla} is the bond length alternation, E_{Res} is the aromaticity, E_{θ} is the planarity, E_{Sub} is the contribution of substituents, and E_{int} is intermolecular interactions.¹⁴ Parameters affecting band gap of aromatic linear π -conjugated systems are illustrated in Fig. 4.

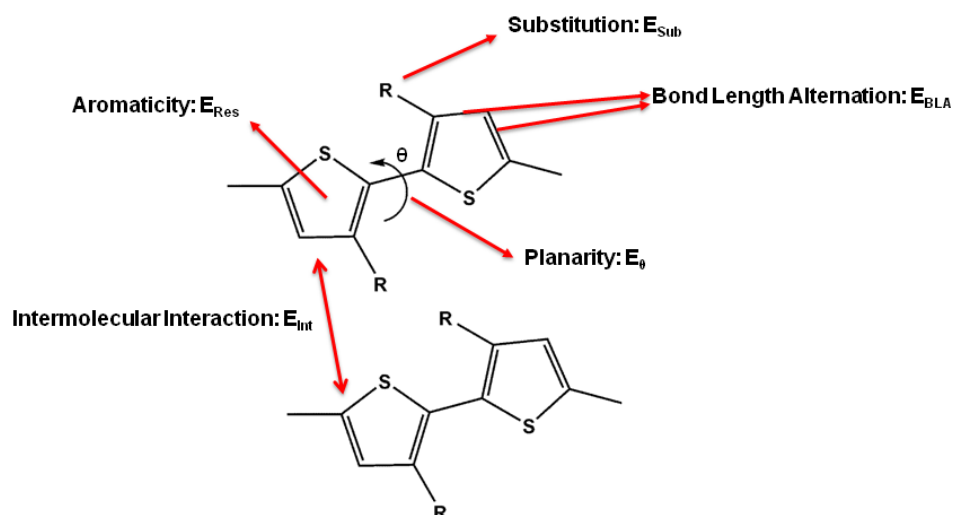


Figure 4. Parameters affecting band gap of aromatic linear π -conjugated systems

1.4.1. Bond Length Alternation

Conductive polymers consist of a serial continuous carbon-carbon double and single bonds.¹⁵ This consecutive structure can be in two different forms named as aromatic and quinoid forms. Aromatic form is obtained with confined π -electrons. Thanks to delocalization of the π -electrons on the polymer backbone, double bonds turn into the single bond form and simultaneously single bonds convert into double bonds. This new structure is called as quinoid form. Bond length alternation (BLA) can be defined as the ratio of aromatic form to quinoid structure which is an important parameter to identify molecular electronic structure and charge transfer characteristics.¹⁶ The more aromatic forms are located on polymer backbone, the higher BLA is attained. Transformation from aromatic form to quinoid form causes BLA to decrease which results with higher energy and narrow band gap.¹⁷

1.4.2. Aromaticity

Increase in aromaticity results in the higher Resonance Energy per Electron (REPE) which causes electron mobility to decrease. Restriction of electron delocalization on

polymer chain causes distortion of the conjugation length therefore band gap of polymer increases.^{18,19}

1.4.3. Planarity

Planarity of the molecule affects the energy levels. Band gap of a polymer can be lowered by increasing planarity of main polymer chain. Planarity of a polymer is necessary for operationalise the p-orbital interactions which enhance the conjugation and electron delocalization on polymer backbone. The tilt angle between rings of neighbour moieties generates E^θ which is under the effect of steric hindrance. Reducing the torsion angle by using different strategies causes increase in conjugation length and decrease in band gap of polymer.^{20,21}

1.4.4. Substituent Effects

Assortment of substituents on a polymer backbone can alter the molecular orbital levels of polymers by changing the electron density on polymer backbone.²² Electron donating group (EDG) causes increase in electron density on π -conjugated system by repelling electrons to polymer backbone which results in the increase of energy of orbitals. This situation facilitates to remove an electron from HOMO. On the other hand, using electron withdrawing group (EWG) as a substituent group lowers the reduction potential and facilitates to movement of electron into LUMO level.²³ In brief, the energy gap between HOMO and LUMO level can be decreased by either substitution of EDG's to increase in HOMO level or using EWG's to lower LUMO level.²⁴

1.4.5. Intermolecular Interactions

Contribution of intermolecular interactions on band gap (E_{int}) arises while polymer chains come together in a material. One individual polymer chain can interact with another chain by secondary forces. Therefore, electron delocalization on polymer

backbone is enhanced and results in the decrease in band gap of the polymer. Solid state materials with more ordered structure and higher crystallinity demonstrates low band gap due to increased π - π stacking and red shift behaviour while comparing with solution state.

1.5. Donor-Acceptor Approach

Donor-Acceptor (D-A) approach is one of the alternative methods to overcome the obstacles of low power conversion efficiency (PCE) by lowering band gap. This theory was firstly proposed by Havinga, Hoeve and Wynberg in 1993.²⁵ In this approach, appropriate electron donor and electron acceptor moieties are produced and combined on polymer backbone to produce D-A or A-D-A type structure. Within this method, band gap of polymer is decreased by hybridization of conduction and valance bands of donor and acceptor units. Combination of electron rich and electron deficient units on polymer backbone creates a new narrow band energy that leads to absorption of longer wavelengths in solar spectrum, enhancement of optical and electrochemical properties and also improvement of exciton charge separation and charge mobility.^{26,27} Creation of new energy levels and band gap for polymer is shown in Fig. 5.

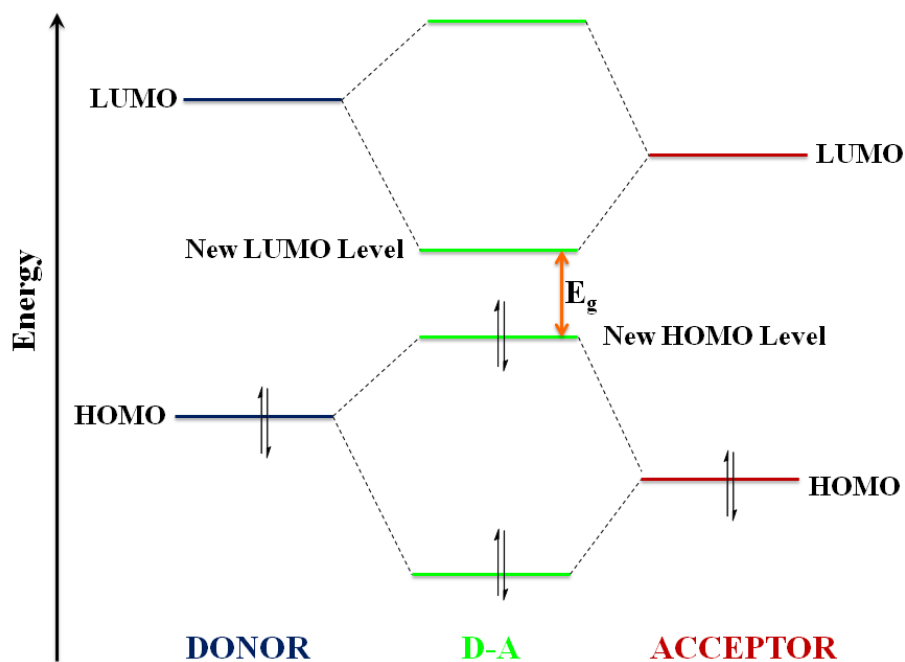


Figure 5. Formation of new HOMO-LUMO energy levels and band gap

1.6. Synthesis Methods for Conjugated Polymers

Polymerization of conductive polymers can be achieved by different techniques. Two of the most popular techniques are electrochemical and chemical polymerization. Both procedures are separated into different sub-methods that affect different properties of polymers such as electronic properties, crystallinity, chain structure or conducting ability. Chemical polymerization technique differs from its electrochemical counterparts with its earthliness to mass production. Although electrochemical polymerization is a rapid mechanism, chemical polymerization provides opportunity to change parameters such as temperature or solvent type to tune properties of the synthesized polymers.²⁸

1.6.1. Electrochemical Polymerization

Electrochemical polymerization is occurred by oxidation of monomers with applied potential. In order to oxidize monomers, an inert indium tin oxide (ITO) coated glass surface is utilized as working electrode. Polymerization process starts with production of radicals by oxidation of monomer. This process was followed by the coupling reactions either between radical and monomer molecule or between two radical cations to produce natural dimer units. This procedure continues with the oxidation of dimer by applied potential and then coupling of produced dimers to form trimers. As successive electrochemical-chemical reactions and rapid growth in length progresses, solubility of produced oligomers decrease and desired product precipitates on working electrode. Due to the fact that an electron transfer (E) is instantly followed by a chemical reaction (C) and then another electron transfer (E) occurs behind, this procedure is called “ECE” mechanism.²⁹ Electrochemical polymerization process of thiophene unit is depicted in Fig. 6.

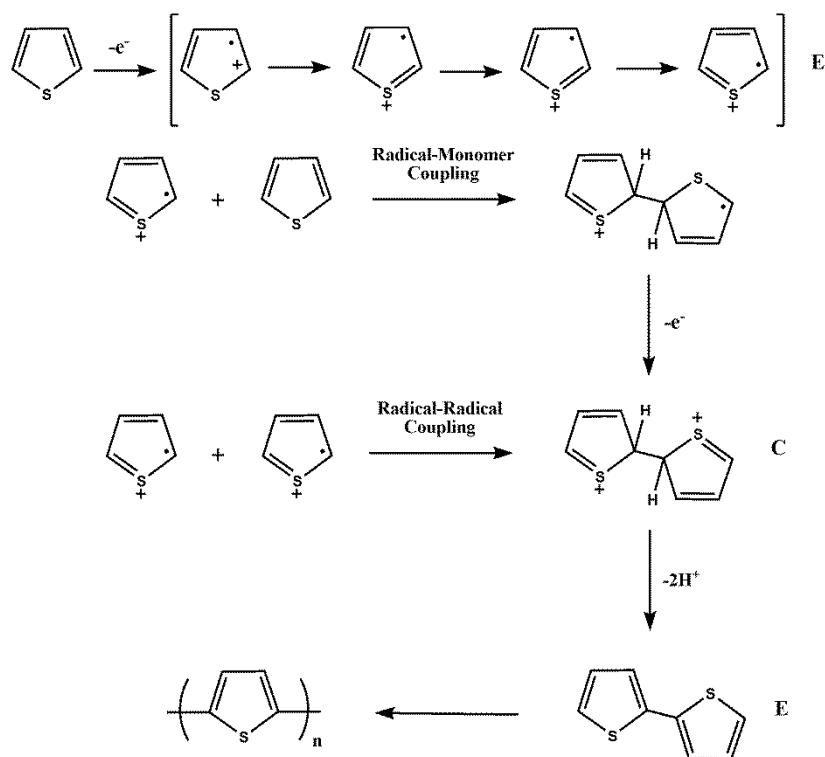


Figure 6. Proposed electrochemical polymerization mechanism of thiophene

Electrochemical polymerization offers great opportunities including potential and thickness control during the polymer synthesis. Because of these properties, electrochemical polymerization technique is favourable for the application of polymer film electrode, thin layer sensor or micro-technological devices.³⁰

1.6.2. Chemical Polymerization

Conjugated polymers are generally synthesized by using two chemical polymerization methods; oxidative polymerization and metal catalyzed coupling reactions. Oxidative polymerization methods are applicable for many aromatic compounds including aniline, pyrrole, phenols, diphenyl sulfide, thiophenols, and thiophene.³¹ Oxidative ferric polymerization also known as Sugimoto method occurs by FeCl_3 as an oxidant at the point where H is bounded. Therefore, active groups like stannyl or halide units are not required for this kind of polymerization processes. Oxidative polymerization procedure with FeCl_3 is generally followed for obtaining high molecular weight polymers with higher purity.

Transition metal catalyst coupling reactions are influential production methods for coupling monomers to produce extended conjugated polymers.³² Kumada, Heck, Negishi, Sonogashira, Suzuki-Miyaura and Stille coupling reactions can be given as main transition metal catalyst carbon-carbon bond formation reactions for synthesis of π -conjugated systems. Richard Heck, Ei-ichi Negishi and Akira Suzuki were granted Nobel Prize in Chemistry Award in 2010 for their publication of ‘‘Palladium catalyzed cross coupling reactions in organic syntheses’’.³³

The synthetic mechanism of palladium catalyzed cross coupling reactions starts with the decomposition of the catalyst ML_n where M represents the metal usually Nickel and Palladium and L symbolizes the ligand. After the separation, with its two attached ligand more reactive catalyst is obtained by reduction of Palladium from Pd

(II) to Pd (0). After that, oxidative addition of organo halide compound to Pd (0) causes formation of Pd (II) active species. In the next step of the reaction, transmetallation occurs with the change of location of organometallic reagent from metal to Pd (II) complex with halide unit. Afterwards, reductive elimination reaction between ligand with Pd (II) and components happens to produce desired product and starting state Pd (0) catalyst. The synthetic mechanism of palladium catalyzed cross coupling reactions is given in Fig. 7.

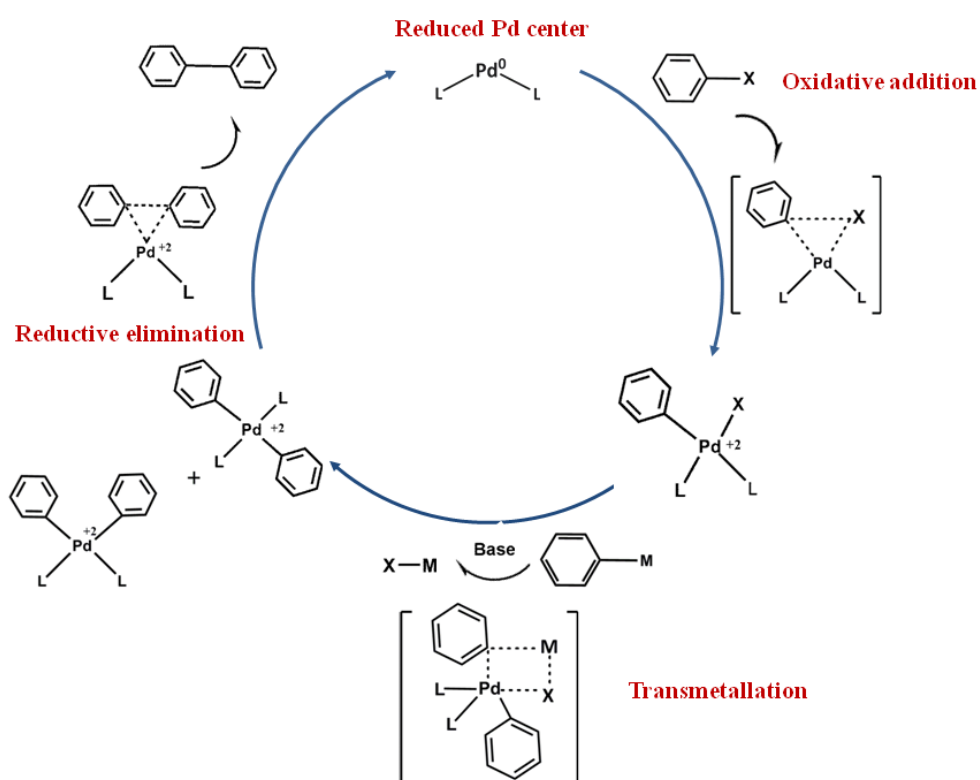


Figure 7. Synthetic mechanism of palladium catalyzed cross coupling reactions

1.7. Moieties in Donor-Acceptor Approach Conjugated Polymers

1.7.1. Quinoxaline Moiety

Quinoxaline moieties are aromatic heterocycles formed by combination of benzene

and pyrazine rings. Their imine nitrogens on pyrazine ring make quinoxaline derivatives strong candidates for using as acceptor units. Also, they demonstrate high electron transporting ability thanks to their two electron withdrawing imine bonds. Possibility of functionalization on both benzene and pyrazine ring leads not only to arrange electron withdrawing character of quinoxaline units but also to increase the solubility character of affiliated D-A type copolymer. Quinoxaline based polymers have been used in many applications such as OPV³⁴, OLED³⁵ and OFET³⁶.

1.7.2. Benzotriazole Moiety

Benzotriazole moieties are heterocyclic molecules containing benzene and aromatic heterocyclic structure. First benzotriazole bearing polymer was achieved by Tanimoto and Yamamoto. This unit plays an important role in photovoltaic studies due to its ascendant electrochromic and photovoltaic properties. Many BTz derivatives are proper for single layer electrochemical devices due to their switching ability between multicoloured and transmissive state.³⁷ In addition to its usage in electrochemical devices, BTz units have high demand in photovoltaic applications because placing a benzotriazole in polymer chain results with low-lying LUMO and n-dopable character.^{38,39,40} They demonstrate strong electron transporting ability thanks to electron withdrawing nature of imine bond. In addition, solubility of final polymer product can be enhanced by long alkyl chain substitution on nitrogen position of Btz. Also, easy modification of N-H bond of BTz unit provides the improvement of structural and electronic properties for good processing ability BTz containing polymers.⁴¹

1.7.3. Benzodithiophene Moiety

Benzodithiophene unit is a symmetrical and planar molecule that consists of the structure of benzene with coherent thiophene. BDT moiety demonstrates excellent electron donor property due to its planar conjugated structure that has the ability to generate π - π stacking easily and increases the charge carrier mobility.⁴² Its structure provides low-lying highest occupied molecular orbital (HOMO) level.⁴³ Besides,

alkyl or alkoxy substituent assigned to BDT derivatives increase the solubility of the polymer in various organic solvents.^{44,45}

1.8. Applications of Conducting Polymers

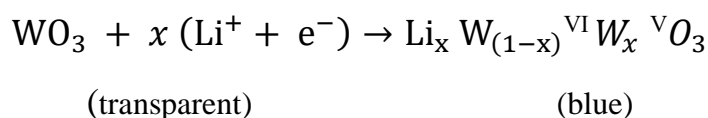
Since their discovery in 1977, conductive polymers (CPs) have gained immense interest due to their numerous advantages compared with its non-conducting counterparts.⁴⁶ These promising materials come into prominence with their low cost, flexibility, stability and conductivity, as well as their electronic and optical properties. They have been preferred in the application of supercapacitors with their higher conductivity ability and greater power capability as compared to inorganic battery materials.⁴⁷ Plastic electronics prevail among electrochromic devices (EC) such as switchable windows and electrochromic mirrors.^{48,49} CPs have been used for the fabrication of Field Effect Transistors (FET) since 1983.⁵⁰ In organic light emitting diodes (OLEDs), emitting layer includes the conducting polymer.⁵¹ Finally, the active layer of organic solar cell devices includes the conjugated polymer as a donor material.⁵²

1.9. Electrochromism

Chromism basically can be defined as the reversible response of a material to an applied external stimulus by color change and this phenomenon has been studied since before the 1900s.⁵³ On the basis of the type of applied stimulus, chromism can be classified as photochromism, thermochromism, ionochromism, halochromism, solvatochromism, electrochromism and so on. Among them, electrochromism is the reversible and observable color change caused by applied potential. Applying potential to electrochromic materials causes to reversible and visible optical change thanks to oxidation- reduction reactions occurred in medium. Upon oxidation and reduction processes, materials exhibit new absorption bands resulting in the demonstration of different colors. Change in colors can take place either between two

different colored states or between a color state and transparent state. Formation of more than one redox states results with generation of number of colors that is termed as multi-chromism.

Electrochromism in inorganic systems consist of thin film states of metal oxides including cobalt oxide, indium tin oxide, iridium oxide, molybdenum trioxide, nickel oxide, tungsten trioxide and vanadium oxide. Intervalance charge transfer properties of metal oxides lead to intense absorption that enhance electrochromic properties of this kind of materials. Among them tungsten trioxide (WO₃) has been gained interest since its discovery in 1969 by Deb.⁵⁴ Then, with its cathodically coloring property WO₃ was utilized in many electrochromic device technologies including electrochromic mirror and smart windows.^{55,56} Metal cations including Li⁺ and H⁺ play a part in proposed mechanism. For example, electrochemical reaction equation with Li⁺ altered between transparent and blue colored state can be written as following.



Viologens are another type of electrochromic materials discovered by Michaelis that can be called also with its long title as 1,1'-disubstituted 4,4'-bipyridinium ions.⁵⁷ During the redox processes of viologens, two different redox states are observed. First step includes a reversible reaction procedure that continues without any variation or side reaction and process continues with less reversible reduction step. The redox procedure of viologens was demonstrated in Fig. 8 where R can be an alkyl, cyclo-alkyl or other side group. Viologen electrochromism offers advantage of tuning structural, electronic and optical properties by changing substitution of molecule. Substitution of different groups affects not only the color of electrochromic system but also solubility of corresponding molecule.⁵⁸

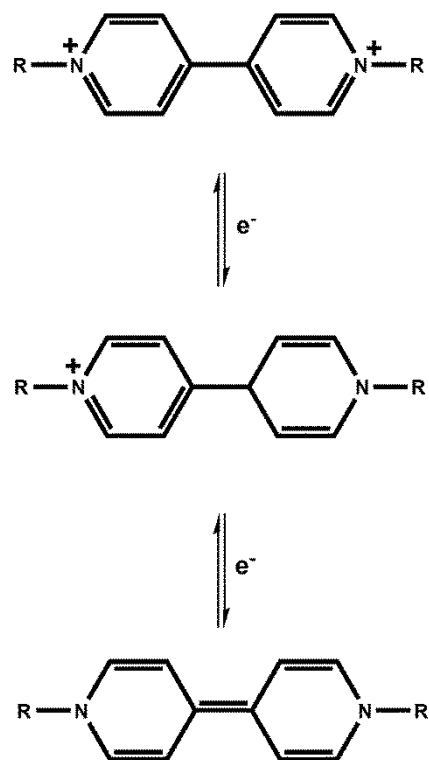


Figure 8. Oxidation-reduction process of viologens

Another type of electrochromic materials are the conductive polymers (CP) that have a leg up on their competitors due to ease of processability and color diversification by alteration of polymer structure with monomer modification or arrangement of polymer backbone.⁵⁹ These organic macromolecules can be synthesized by either chemically or electrochemically. Actually, conducting polymers are insulators in their neutral states and gain conductivity through doping mechanism that causes to enhancement of optical and electronic properties by the formation of different charge carriers such as polarons and bipolarons in medium. Thus, doping-dedoping process is the principal source of electrochromic behaviour of these organic aromatic molecules.⁶⁰

All optical properties especially colours of conducting polymers are directly bounded up their band gap energy that is the difference between HOMO and LUMO levels.

Substitute groups of repeating units play a crucial role on energy levels and band gap of conjugated polymers by affecting structural and electronic properties including planarity or conjugation length. By constructing polymers with considerable substituents, band energy of a conducting polymer can be tuned and desired color can be achieved. Addition of an electron rich moiety on polymer chain which leads to increase in HOMO energy level and addition of electron deficient unit that causes to decrease in LUMO level results with the change in band gap and absorption behaviour results with red and blue shift on spectra.⁶¹

1.9.1 Parameters Affecting Electrochromic Devices

1.9.1.1. Optical Contrast

Electrochromic contrast which is also called as percent transmittance change at defined wavelength or a range (%T) is the essential parameter to appraise the electrochemical properties of a material. Fluctuation of percent transmittance is reported at the highest contrast. For obtain reliable data, change in luminance value is measured for electrochromic contrast value because it gives information about transmissivity of corresponding material.⁶²

1.9.1.2. Coloration Efficiency

Coloration efficiency is the measurement of necessary power amount for an electrochromic material. In other words, coloration efficiency is the numerical measure of observed color of electrochromic systems.⁶³ While some electrochromes exhibit intensive color with potential applied, others show lighter tones. Coloration efficiency is the parameter that defines the differences between these materials. Coloration efficiency depends on the charge density and can be determined as following equation:

$$\eta = \frac{(\Delta OD)}{Q_d} = \frac{\log \left[\frac{T_b}{T_c} \right]}{Q_d}$$

Where η is the coloration efficiency at a specific wavelength, ΔOD is optical charge density change, Q_d is the ratio of electronic charges, T_b and T_c are the transmittance values of oxidized and reduced forms.

1.9.1.3. Switching Time

Switching time is the duration passing between colored and bleached states or two colored states of electrochrom. Many conditions including ion conductivity, ion diffusion in film, amount of applied potential, thickness of electrochromic material and morphology affects the switching speed of EC material. For many applications such as switchable windows or displays, switching time is an important parameter to provide fast response for used devices.⁶²

1.9.1.4. Optical Memory

The time for an electrochromic material maintains its color after withdrawing applied potential is described as optical memory. It should be long enough not only to sustain the stability of device but also to economize energy consumption.

1.9.1.5. Stability

Stability of an electrochromic device is measured by its durability along electrochemical processes. Degradation of oxidation-reduction couple causes to lack of electrochromic properties of the material. Degradation usually takes place due to irreversible redox reactions; iR losses of electrode and electrolyte; water and oxygen containing cells and heat release from resistive parts.⁶²

1.10. Organic Solar Cells

Organic solar cells (OCSs) are devices with organic semiconductor active layer utilized for the formation of electricity from sunlight. With the increase of energy demand, interest in OSCs has been gathered speed in both industry and academia due to their application to large areas, flexibility and low cost. This type of energy sources offer access to clean, cheap and renewable energy with ease of device fabrication procedure. When comparing with their inorganic counterparts, they exhibit higher absorptivity and thinner device structure. However, low rate of converting sunlight to electricity which is called as power conversion efficiency (PCE) for a cell is the main drawback of the organic solar cells. Studies have been performing to provide increase in power conversion efficiency of OSC's. Different device architectures are constructed to produce more efficient organic solar cells with enhancing light absorption or exciton diffusion.⁶⁴

1.10.1. Device Architecture of Organic Solar Cells

1.10.1.1. Bilayer Solar Cells

First bilayer solar cell structure was constructed by Tang et al in 1985 which differs from single layer device architecture in that the active layer sandwiched between two electrode includes two different conducting material. Structure of this novel device was composed of ITO coated glass, copper phthalocyanine (CuPc), perylene tetracarboxylic derivative, opaque Ag layer respectively from top the bottom.⁶⁵ In general, a bilayer solar cell has a device fabrication arrangement as anode/hole connection layer/two separated active layer including donor and acceptor/electron collecting layer/cathode. The most important disadvantage of bilayer type of solar cells is the limited exciton diffusion length that prevents the modification of device thickness. In the case of thick donor- acceptor unit, arrival of exciton gets difficult due to the long distance between heterojunction area and corresponding unit. To compensate this drawback, active layers are prepared thinner which causes another

problem of low absorption of light for solar cell. All these unfavourable conditions affects the efficiency of formation of electricity from sunlight.⁶⁶

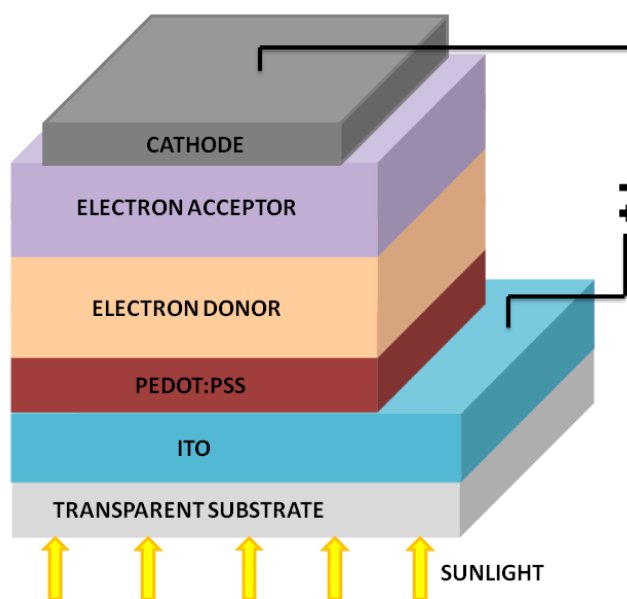


Figure 9. Bilayer heterojunction solar cell device structure

1.10.1.2. Tandem Solar Cells

First organic tandem solar cell was invented by Hiramoto et al. in 1990 with the purpose of increase efficiency through the combination of two or more solar cell system with different band gaps, absorption ability and charge carrier ability. This construction was included two small molecule-based cells coupled in series with the p-n junction of metal-free phthalocyanine and perylene tetracarboxylic derivative. The contact between two cells was provided by evaporated Au and satisfactory V_{oc} result was achieved as two times more than the single cells.⁶⁷ Basically a tandem solar cell is composed of ITO coated glass, bottom device, intermediate layer such as Au or Ag, top device and top electrode. Definitely, the most critical benefit of tandem solar cell is the harvesting of sunlight more effective which enhances

efficiency of the solar cell.⁶⁸ Tandem solar cell device structure is depicted on Fig. 10.

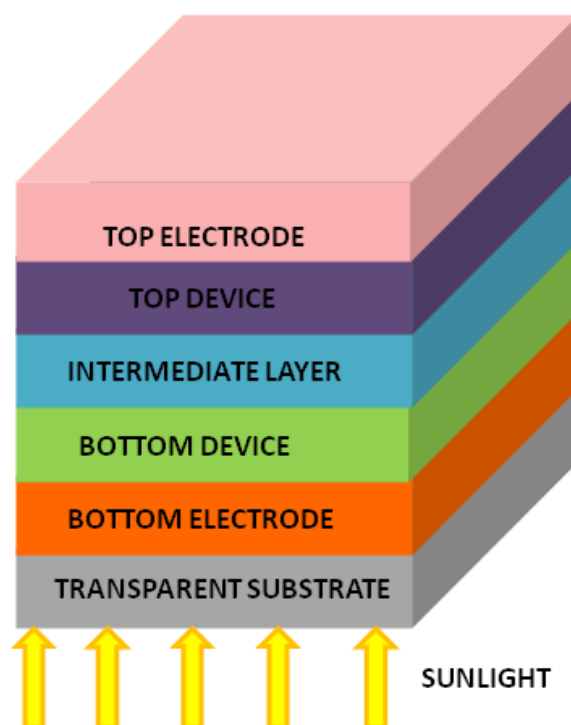


Figure 10. Tandem solar cell device structure

1.10.1.2. Bulk Heterojunction Organic Solar Cells

Bulk Heterojunction (BHJ) organic solar cells are devices that include a physical blend of donor and acceptor material in their active layer. The first BHJ polymer solar cell was constructed in 1995 by Heeger et al. including poly[2-methoxy-5-(2-ethylhexyloxy)1,4-phenylene vinylene] (MEH-PPV) as a donor and phenyl [6,6] C₆₁ butyric acid methyl ester (PCBM) as an acceptor unit that exhibits great efficiency results when compared with bilayer counterparts.⁶⁹ The main cause of the improvement of efficiency is the formation of a larger bicontinuous interface between donor and acceptor units which offer a shorter travel distance to produced excitons. On the contrary of bilayer solar cells, in BHJ solar cells, the random composition of donor-

acceptor interface interact with both anode and cathode that could be results with the unfavourable charge collection. To inhibit this situation, transition interfacial layers including hole transport layer and electron transport layer were located between electrode and active layer.⁷⁰ Generally, active layer of a bulk heterojunction cell includes the combination of p- type conjugated polymer as donor unit and n- type fullerene derivative as an acceptor. Device fabrication involves firstly coating of PEDOT: PSS as hole transport layer on ITO surface, covering polymer-PCBM blend on this layer and evaporation of cathode material on active layer. Bulk Heterojunction device architecture is displayed on Fig. 11.

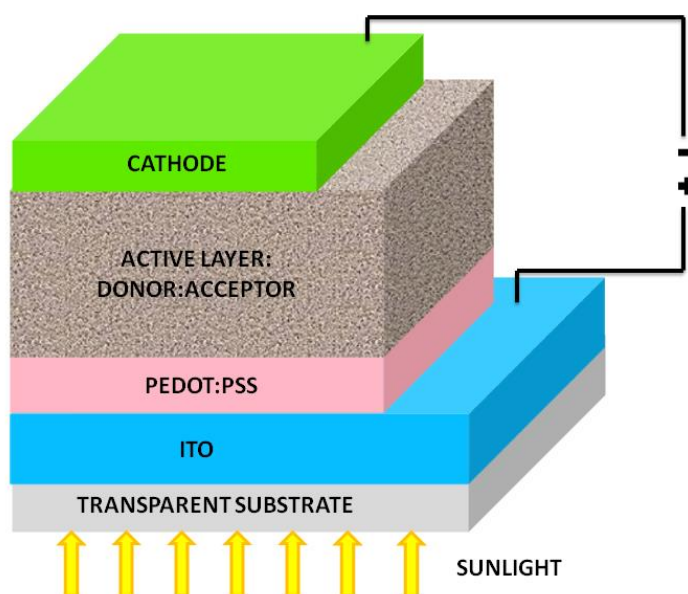


Figure 11. Device architecture of bulk heterojunction solar cell

1.10.2. Mechanism of Organic Solar Cells

Energy production from light can be divided into four basic steps including light absorption and exciton generation, exciton diffusion, charge separation and charge extraction as shown in Fig. 12. Firstly, light absorption occurs from the active layer

of the solar cell, which causes to production of bounded electron-hole pair called as exciton. Exciton is formed due to low dielectric constant resulting with strong Coulombic attraction between hole and electron although absorption of a photon is ended with the exciting of electron from VB to the CB for inorganic semiconductors. Later, exciton diffusion step takes place containing only the transportation of bounded pair from donor to the donor- acceptor interface. Most important issue about this stage is the exciton diffusion length (L_D) which could be defined as the lifetime of an exciton. For an exciton in a polymeric system, diffusion length is about 1-10 nm. At donor-acceptor interface, because of the high energy difference between LUMO of the donor and acceptor units each charge goes towards to the corresponding electrode and charge separation is accomplished. Then, charge extraction stage occurs including hole transportation to the anode and electron movement the cathode. Efficiency of the charge transfer is related with the electrical conductivity and impedance of the organic materials. Due to the arrival of the charges to corresponding electrodes, electricity is produced by completing the overall cycle.^{9,71,72}

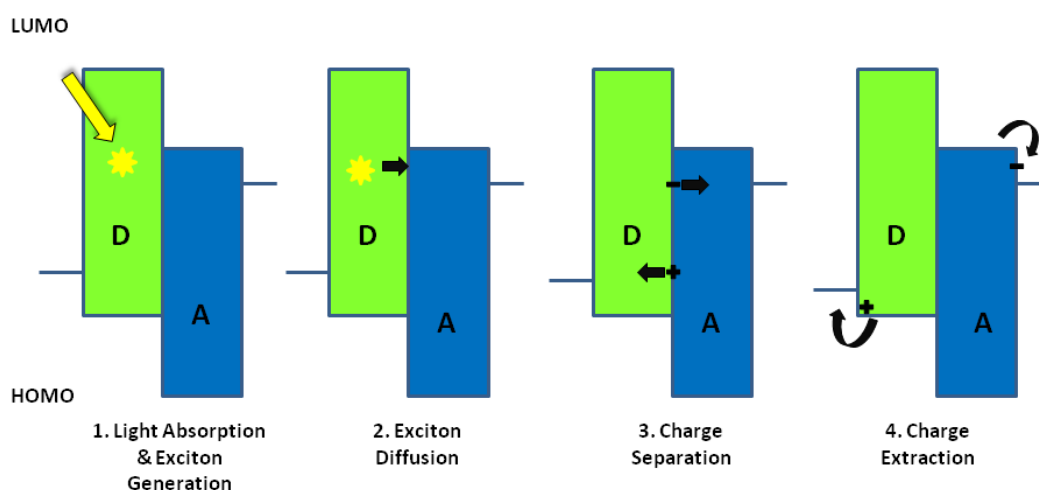


Figure 12. Working principle of organic solar cell

1.10.3. Characterization of a Solar Cell Device

Characterization of an organic solar cell is performed from its current density-voltage (J-V) curve drawn under the illumination of 1 kW/m² light at an incident angle of 48.2°. These illumination standards called as Air Mass 1.5 Global (AM 1.5 G) are determined considering the reduction of solar power by external factors including reflection, scattering or absorption by atmospheric elements and the incidence angle of the sunlight. In general, air mass is the measurement of the amount of sunlight attained to the earth. Specifically, international AM 1.5 spectrum of radiation is chosen for solar cell studies.

Measurements are made under two different conditions including dark and illumination. In the dark, current does not flow throughout the device and graph line crosses over the origin. On the other side, under illumination system generates power and J-V curve is located at the IV. quadrant of the graph. Typical current- voltage characteristics of an OSC under two conditions are illustrated in Figure 12. The point that highest current and voltage obtained is called as maximum power point (MPP). I_{mpp} and V_{mpp} represent the points where current and voltage show the maximum values. Efficiency of an organic solar cell is defined as power conversion efficiency (η_e) and calculated by following equation:

$$PCE = \frac{V_{OC} \times J_{SC} \times FF}{P_{in}}$$

Where η_e is the power conversion efficiency (PCE) of solar cell, J_{sc} is short circuit current, V_{oc} is open circuit voltage, P_{in} is the incident light and FF is the fill factor. All these factors influence the PCE of solar cell and studies have been conducted to increase efficiency with increasing all these factors.^{73,74}

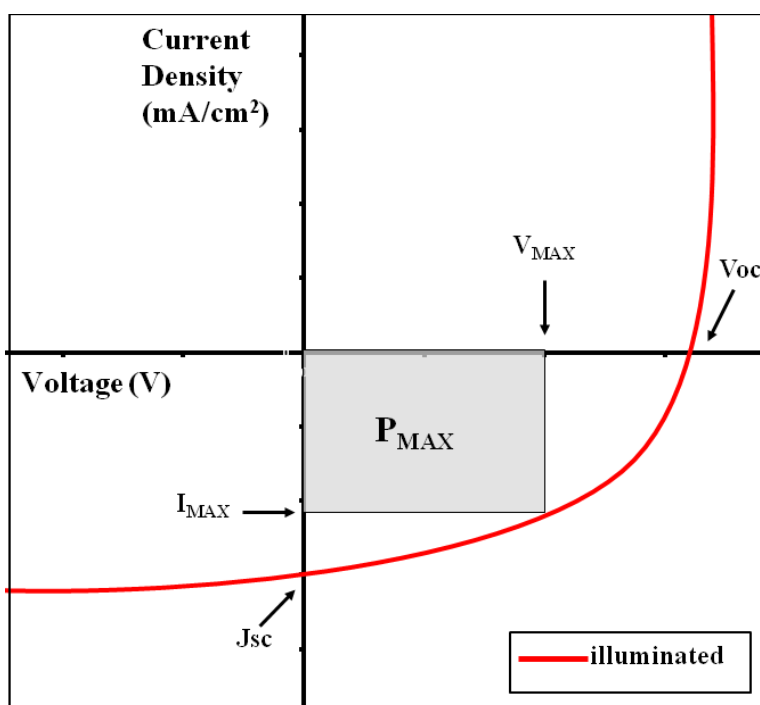


Figure 13. Current density-voltage characteristics of OSC under dark and illumination

1.10.4. Basic Factors Affecting Efficiency of an Organic Solar Cell

1.10.4.1. Open Circuit Voltage

As discussed earlier in section 1.10.2. process of electricity production via sunlight is composed of four basic steps consisting light absorption and exciton generation, exciton diffusion, charge separation and charge extraction. In exciton diffusion step, charge carriers travel to the respective electrodes with diffusion phenomenon under the influence of built-in potential. Under open circuit condition and steady state illumination, transportation of charge carriers to anode and cathode creates a potential difference between two electrodes and counteract the influence of built-in potential. In such a case, carrier generation and recombination counterpoise each

other and extinguish the current flow through the device. This situation is called as ‘quasi equilibrium state’ and potential difference between electrodes is known as the open circuit voltage (V_{OC}). V_{OC} could be defined as the highest voltage value of the cell can produce to external load.⁷⁵

Various studies were made to understand the effect of V_{OC} on efficiency of a solar cell. In the light of information from studies conducted by Brabec and Scharber, it is defended that V_{OC} of an OSC directly depends on the LUMO energy level of the acceptor and also HOMO energy level of the donor. Relationship between V_{oc} and HOMO-LUMO energy levels were proposed by the following equation:

$$V_{oc} = \frac{1}{e}(E^{Donor}HOMO - E^{Acceptor}LUMO) - 0.3 V$$

Where e is the elementary charge, $E^{Donor}HOMO$ is the HOMO level energy of the donor and $E^{Acceptor}LUMO$ is the LUMO level energy of the acceptor.⁷⁶

1.10.4.2. Short Circuit Current

Short-circuit current (J_{SC}) is known as the current generated by solar cell device under illumination without applying external potential. J_{SC} of an OSC device can be calculated by the following equation:

$$J_{sc} = ne\mu E$$

Where n is the density of charge carriers directly depends on the band gap of corresponding polymer that employed to absorption of the solar spectrum. Charge carrier mobility is symbolized with μ in the equation and can be enhanced with a structured morphology of organic thin film. Also, e is the elementary charge and E corresponds to the electric field.^{70,73}

Electrical current of a solar cell device is equal to the population of the collected charges at electrodes. Count of the charges at electrodes depends on the efficiency of all five stages which an exciton passes along its journey from active layer to the electrodes. External quantum efficiency (EQE) is the combination of the all efficiencies of these stages which could be described as the ratio of the number of incoming photons to the count of the produced charges. EQE can be estimated by the following formula.

$$EQE = \eta_a * \eta_{edf} * \eta_{ds} * \eta_{ct} * \eta_{cc}$$

Where η_a is the absorption efficiency, η_{edf} is the electron-hole pair diffusion efficiency, η_{ct} is the efficiency of the migration of charges, η_{ds} is the dissociation efficiency of the exciton and η_{cc} is the effectivity of the charge collection.⁷⁷ Occasionally, EQE is referred as incident photon conversion efficiency (IPCE) which can be calculated by the equation below:

$$IPCE = \frac{1240 J_{sc}}{\lambda P_{in}}$$

Where J_{sc} is the short circuit voltage, λ is the wavelength of the incident photon and the P_{in} is the power available in the incident solar radiation.⁷⁸

1.10.4.3. Fill Factor

Fill factor (FF) is the principle parameter of product of the efficiency which is the blended conclusion of the different stages of the energy production from exciton formation to the charge collection. Fill factor mainly describes how easily or difficultly charge carriers can be originated out of the photovoltaic cell. Stated in other words, FF expresses how executed performance filled the ideal performance of the solar cell. Fundamentally, FF is the measurement of the squareness of the J-V curve which corresponds maximum value as 100% when makes an ideally perfect

rectangular shape.⁷⁹ FF of an organic device can be estimated by the following formula:

$$FF = \frac{V_{max} J_{max}}{V_{oc} J_{sc}}$$

Where V_{MAX} - J_{MAX} are the voltage and current values at P_{MAX} which describes the realistic performance of the device, V_{oc} and J_{sc} are the open circuit voltage and short circuit current values that belong to ideally achievable performance of the device.⁸⁰

1.11. Quinoxaline Containing Polymer Solar Cells

For design of the novel D-A type polymers, quinoxaline moieties are utilized in polymer backbone thanks to their interesting optoelectronic properties. With its strongly electronegative imine groups, relatively stable quinoid form and high solubility property, quinoxaline unit is one of the most popular acceptor moiety candidate to achieve low band gap conjugated polymers.^{81,82,83} Furthermore, quinoxaline units offer the possibility of tuning electron withdrawing character by introducing substituent groups either on the benzene or on the pyrazine ring.^{84,85} Therefore, they are combined with different electron rich donor groups such as benzodithiophene, carbazole and fluorine to obtain solar cells with high PCE.^{86,87,88}

Among these donor units, BDT demonstrates good electron donor property. Its benzene coherent thiophene structure provides low-lying HOMO level, which enhances the V_{oc} and also PCE. In literature, quinoxaline and BDT containing polymers achieve high PCE as a result of high V_{oc} .^{89,90} In 2008, Hou et al. reported that 4,8bis(dodecyloxy)benzo[1,2b:4,5b']dithiophene and 2,3- diphenylquinoxaline containing polymer **H1** (Figure 14) demonstrated %0.23 PCE and V_{oc} , J_{sc} , and FF of the device were estimated as 0.60 V, 1.53 mA/cm² and 26% respectively by using 1:1 (w:w) polymer/PCBM ratio.⁹¹ On the other hand, study which was published at

2012 by Fu et al. showed that modification of the benzene rings on the quinoxaline units enhances the PCE of polymer. In this study, 5,8-dibromo- 2,3-bis(4-(octyloxy)phenyl)quinoxaline and 2,6-bis(trimethyltin)-4,8-bis (2-ethylhexyloxy)benzo[1,2-b:4,5-b']dithiophene units were polymerized and produced polymer **P(BDT-Qx)** (Fig. 14) shows 1.9% PCE with V_{oc} as 0.77 V, I_{sc} as 5.0 mA/cm² and FF as 50.3% . In 2013, a study was published by Kim et al. that includes the polymerization of 8,11-Dibromobenzo[a]phenazine unit with 2,6-Bis(trimethylstannyl)-4,8-bis(2-ethylhexyloxy)benzo[1,2-b:4,5-b']dithiophene by following Stille coupling reaction procedure. With using the device configuration of ITO/PEDOT: PSS /polymer:PC₇₁BM (1:1.5 wt %)/Ca/Al, **PBDT-DBPz** (Figure 14) showed maximum PCE value as 2.01%.⁹² However, same donor structure was polymerized with 5,8-Dibromo-2,3-bis(5-octylthiophen-2-yl) quinoxaline by Gongs' group and PCE of **PBDTThQx** (Figure 14) was found as 0.74%.⁹³

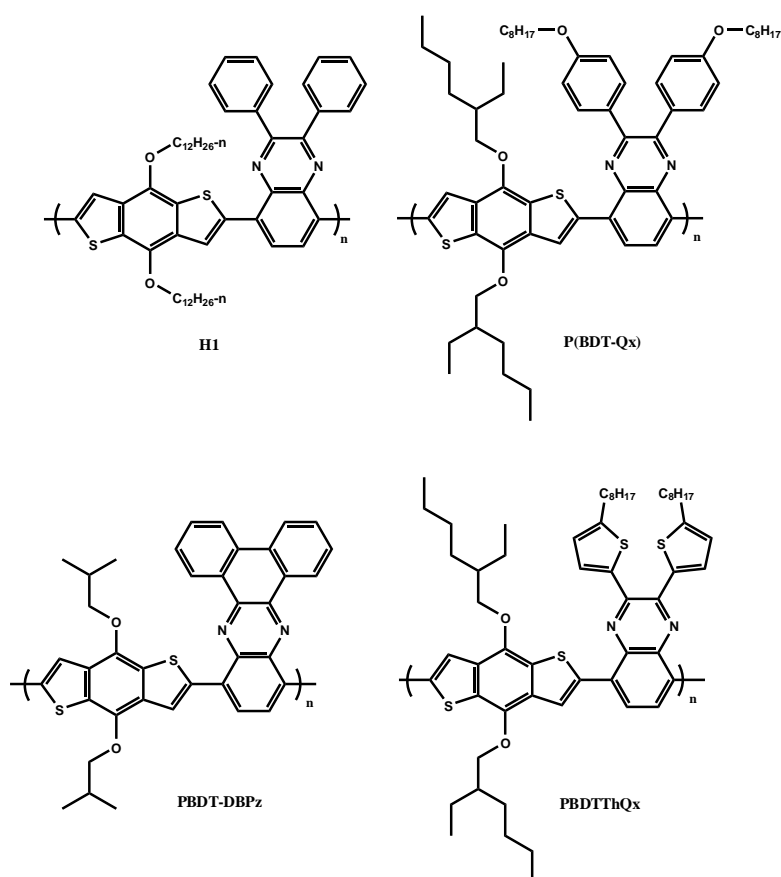


Figure 14. Structures of H1, P(BDT-Qx), PBDT-DBPx and PBDTThQx

Also, BTz is the another acceptor moiety utilized in many photovoltaic applications since placing a benzotriazole in polymer chain results with low-lying LUMO and n-dopable character.^{39,40} This moiety demonstrates strong electron transporting ability thanks to electron withdrawing nature of imine bond.⁹⁴ Solubility of the polymer can be increased by long alkyl chain substitution on nitrogen position of Btz.⁹⁵ Solubility of a polymer is a crucial parameter for not only to ease purification steps but also to produce high quality thin films for device application.⁹⁶ In light of these valuable properties, benzotriazole derivatives were used in many photovoltaic applications. Cevher et al. combined BTz with quinoxaline on polymer backbone randomly and produced polymers **CoP1**, **CoP2** and **CoP3** demonstrated the best PCE results as 2.13%, 1.72% and 1.54% respectively.⁹⁷ Structures of polymers are given in the Fig. 15.

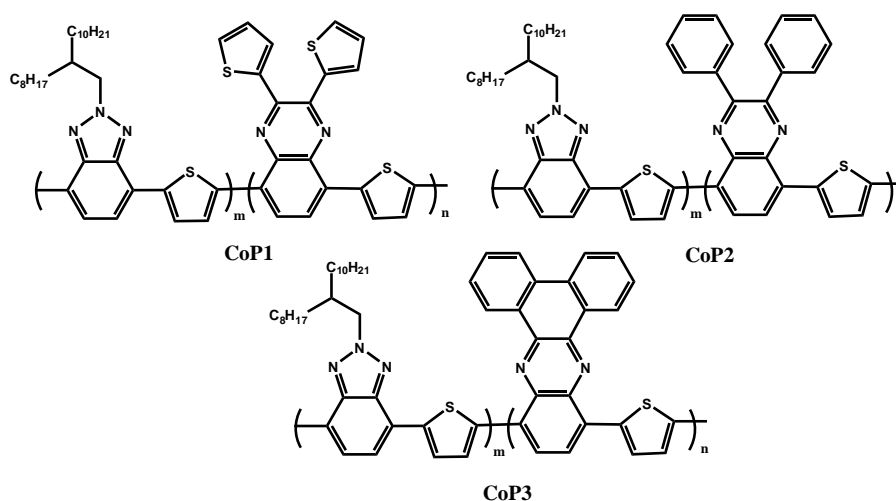


Figure 15. Structure of CoP1, CoP2 and CoP3

1.12. Aim of the Study

Donor acceptor approach is one of the prospering methods to manufacture p-type material for OSC application. In this study, three quinoxaline moieties with different substituents were chosen to combine with BTz and benzodithiophene units randomly

to achieve broad visible light absorption. Broad light absorption can be achieved by covering huge part of visible spectrum. In literature, benzodithiophene and quinoxaline based copolymers demonstrates maximum absorption value around 600-730 nm.^{98,99} Also, copolymers including benzotriazole and benzodithiophene derivatives reveal maximum absorption at around 500 nm.^{100,101} Addition of benzotriazole unit to quinoxaline-benzodithiophene containing polymer backbone atones the lack of absorption of visible region. Herein, 4,7-dibromo-2-(2-octyldodecyl)-2H-benzo[d][1,2,3]triazole and 2,6-Bis(trimethyltin)-4,8-bis(2-ethylhexyloxy)benzo[1,2-b:4,5-b']dithiophene were randomly polymerized by Stille coupling reaction procedure with 5,8-dibromo-2,3-di(thiophen-2-yl)quinoxaline, 5,8-dibromo-2,3-diphenylquinoxaline and 10,13-dibromodibenzo[a,c]phenazine to provide broad visible light absorption with high absorption coefficient that enhances the photon absorption and power conversion efficiency of the OSC devices. Structures of copolymers were indicated below in Fig. 16.

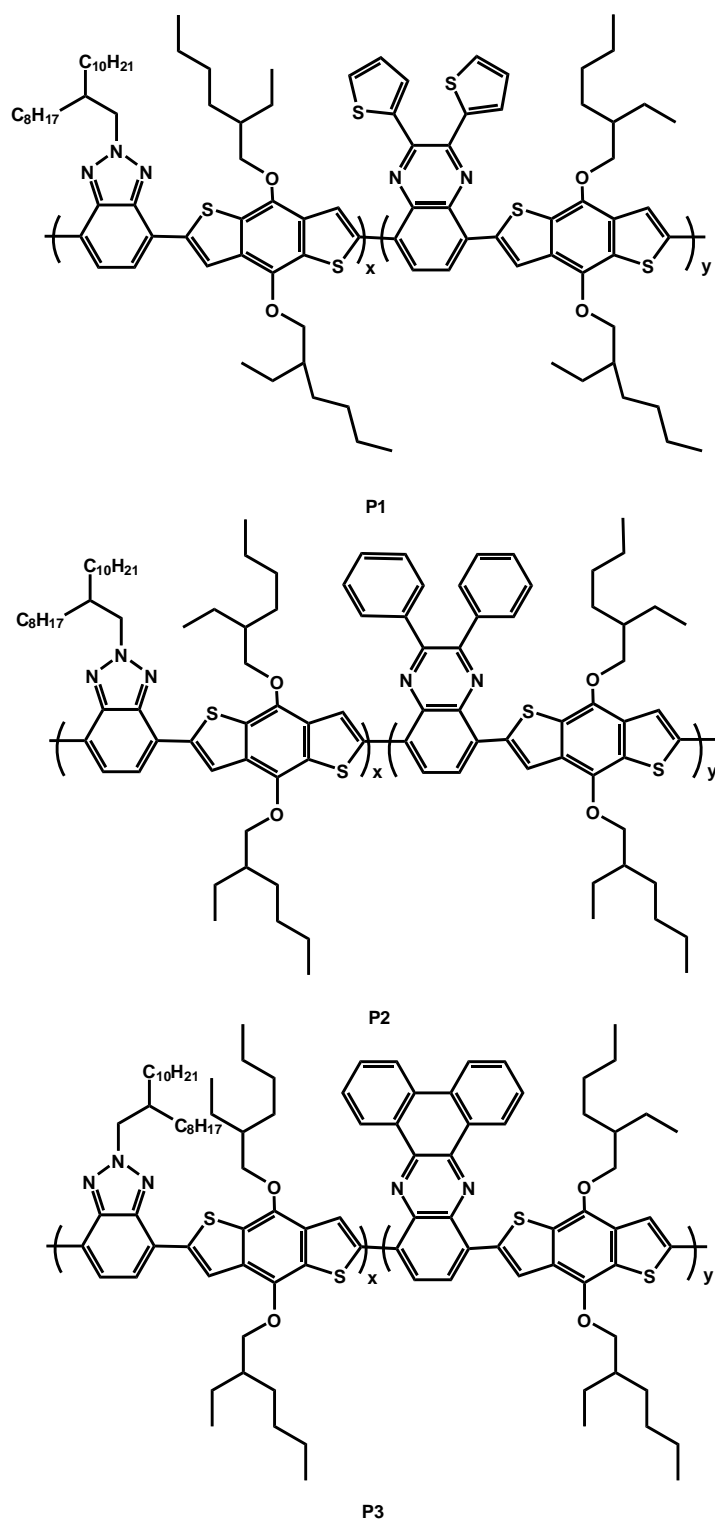


Figure 16. Structure of synthesized copolymers P1, P2 and P3

CHAPTER 2

EXPERIMENTAL

2.1 Materials and Equipments

All expended chemicals and reagents in the synthesis of monomers and polymerization processes were purchased from Sigma Aldrich Chemical Co. Ltd. Metallic sodium and benzophenone were used for the purpose of drying tetrahydrofuran (THF) and toluene. Beside these, solvents were used without any purification or drying steps. PC₇₁BM was purchased from Solenne for solar cell application. Moisture and air sensitive procedures were done under argon atmosphere and the others were carried out under air atmosphere. Column chromatography technique was used for purification process of materials by using Merc Silica Gel 60.

Nuclear Magnetic Resonance Spectroscopy technique was used to confirm chemical structures of both monomers and polymers. ¹H and ¹³C NMR shifts were taken by using Bruker Spectrospin Avance DPX-400 Spectrometer according to trimethylsilane (TMS) internal reference in deuterated chloroform (CDCl₃). For polymers, gel permeation chromatography (GPC) was used to estimate average molecular weights by taking polystyrene standard as reference in chloroform (CHCl₃). Spectroelectrochemical studies of synthesized polymers were done by using Varian Cary 5000 UV-Vis Spectrometer and Minolta CS-100 Spectrometer. For cyclic voltammetry studies, a Gamry 600 potentiostat were used.

Thermal behaviours and properties were examined by using thermogravimetry analysis (TGA) and differential scanning calorimetry (DSC). Heat capacities, melting temperature (T_m) and glass transition temperatures (T_g) were calculated by using Perkin Elmer Differential Scanning Calorimetry with a 10°C/min heating rate up to

950°C. Decrease in polymer weight was calculated by Perkin Elmer Pyris 1 TGA under nitrogen atmosphere with a 10°C/min heating rate to 950°C.

2.2. Synthesis of Monomers

2.2.1. Synthesis of 9-(bromomethyl)nonadecane

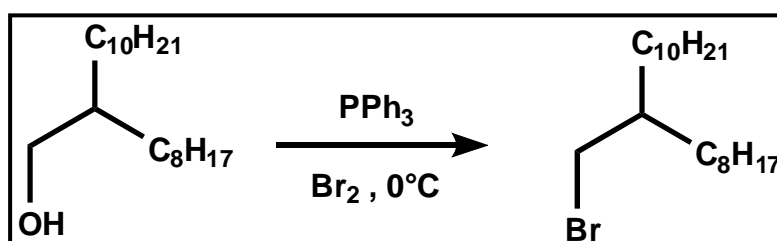


Figure 17. Synthesis of 9-(bromomethyl)nonadecane

2-Octyl-1-dodecanol (5.00 g, 16.65 mmol) was dissolved in 50 mL dichloromethane (DCM) under argon atmosphere at 0°C. After waiting about 15 minutes for dissolving alcohol, addition of triphenylphosphine (PPh₃) (4.60 g, 17.6 mmol) was done and argon was cut. Bromine (2.53 g, 35 mmol) in 5 mL of DCM was added to reaction mixture drop by drop and mixture was stirred about 40 minutes at 0°C. Then temperature was raised to room temperature and stirred overnight. Concentrated NaHSO₃ solution was poured into the reaction mixture to remove excess bromine. Addition of NaHSO₃ solution caused to colour change in solution from dark to the straw yellow. Extraction was performed with DCM and water and lastly organic phase was washed with brine. After, collection of organic phase was dried over MgSO₄. After evaporation of DCM under reduced pressure, snow like white solid was obtained. Purification of obtained solid was occurred with column chromatography technique on silica gel by using hexane. Then, product was obtained as colourless oily liquid. (5.36 g, 89% yield) ¹H NMR (400 MHz, CDCl₃) δ (ppm): 3.37 (d, J = 4.7 Hz, 2H), 1.51 (m, 1.55 – 1.47, 1H), 1.21 (m, 32H), 0.81 (t, J =

6.8 Hz, 6H) ^{13}C NMR (100 MHz, CDCl_3) δ (ppm): 39.5, 34.6, 32.6, 31.9, 31.6, 29.7, 29.4, 26.9, 26.6, 25.3, 22.7, 20.7, 14.1.

2.2.2. Synthesis of 4,7-dibromobenzo[*c*][1,2,5]thiadiazole

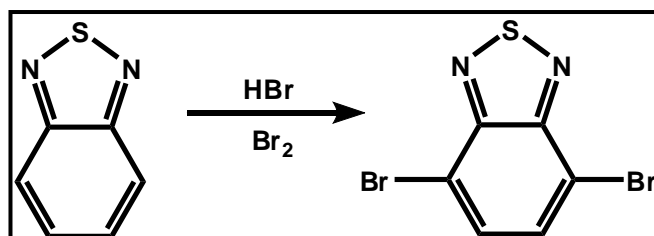


Figure 18. Synthesis of 4,7-dibromobenzo[*c*][1,2,5]thiadiazole

Benzo-1,2,5-thiadiazole (5.00 g, 36.60 mmol) was dissolved in 65 mL of HBr in round bottom flask and reaction mixture was stirred at 90°C about 1 hour. Bromine diluted in 45 mL of HBr was added drop by drop to reaction. After, temperature was raised up to 120°C and reaction was refluxed under argon for 15 hours. Reaction medium was cooled to room temperature and sufficient amount of NaHSO_3 solution was put into the reaction medium to get rid of excess bromine. Reaction was filtered and solid residue was washed with diethyl ether several times. Yellow solid residue was produced, and no further purification technique is needed (10.23 g, 95% yield). ^1H NMR (400 MHz, CDCl_3) δ 7.67 (s, 2H). ^{13}C NMR (101 MHz, CDCl_3) δ (ppm): 152.8, 132.3, 113.8.

2.2.3. Synthesis of 3,6-dibromobenzene-1,2-diamine

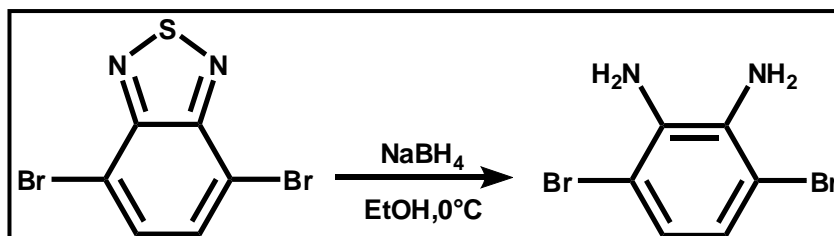


Figure 19. Synthesis of 3,6-dibromobenzene-1,2-diamine

4,7-Dibromobenzothiadiazole (10.30 g, 34.80 mmol) and 300 mL of EtOH was put into reaction flask. After dissolution, mixture was cooled to 0°C in an ice bath. NaBH₄ (32.90 g, 0.87 mmol) powder was added slowly and carefully to the reaction flask. After gas evolution was stopped, temperature was increased to the room temperature and stirred at this temperature about 18 hours. After complete evaporation of EtOH, extraction was performed with diethyl ether and water and collection of organic phases was extracted with brine at final step. MgSO₄ was used for removing residual water. Solvent was evaporated and 3,6-dibromobenzene-1,2-diamine was produced as faint yellow solid (4.90 g, 54% yield). ¹H NMR (400 MHz, CDCl₃), δ (ppm): 6.84 (s, 2H), 3.90 (s, 4H). ¹³C NMR (101 MHz, CDCl₃) δ (ppm): 133.74, 123.26, 109.69.

2.2.4. Synthesis of 4,7-dibromo-2H-benzo[d][1,2,3]triazole

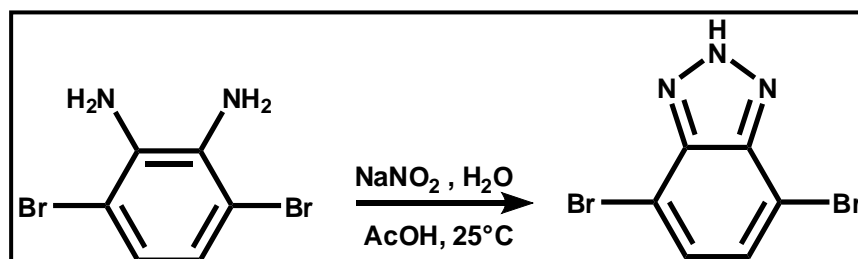


Figure 20. Synthesis of 4,7-dibromo-2H-benzo[d][1,2,3]triazole

3,6-dibromobenzene-1,2-diamine (4.00 g, 15.1 mmol) was dissolved in 75 mL of acetic acid (AcOH) solution. After, NaNO₂ (1.50 g, 16.56 mmol) in 36 mL of water was dropped slowly to the reaction medium and reaction was allowed to stir about 1 hour at room temperature. Precipitate was filtered and rinsed with distilled water several times until the acidic odour was over to produce pink powder. (2.74 g, 66% yield)

2.2.5. Synthesis of 4,7-dibromo-2-(2-(2-octyldodecyl))-2H-benzo[d][1,2,3]triazole

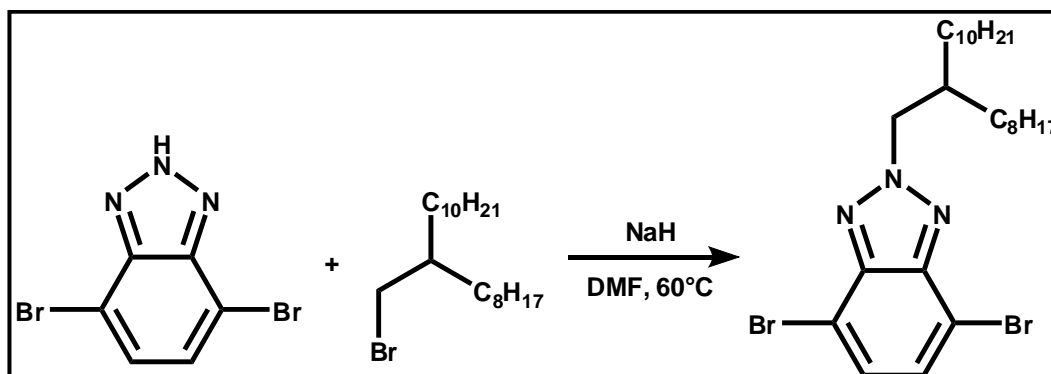


Figure 21. Synthesis of 4,7-dibromo-2-(2-(2-octyldodecyl))-2H-benzo[d][1,2,3]triazole

4,7-Dibromo-2H-benzo[d][1,2,3]triazole (2.74 g, 9.86 mmol) was dissolved in 10 mL of dimethylformamide (DMF) under argon atmosphere. Reaction temperature was reduced to the 0°C before the addition of NaH (0.29 g, 12.06 mmol). After addition of NaH, temperature was elevated to 60°C and 9-(bromomethyl)nonadecane (3.78 g, 10.47 mmol) was added at this temperature. Reaction was stirred overnight at 70°C. After, extraction was done with diethyl ether and brine and organic phase was dried over MgSO₄. Organic solvent was vaporized under reduced pressure and product was obtained as faint yellow oil. Purification was achieved by column chromatography technique on silica gel with hexane and chloroform (1:2) and 4,7-dibromo-2-(2-(2-octyldodecyl))-2H-benzo[d][1,2,3]triazole was obtained as a yellow oil. (2.75 g, 50% yield) ¹H NMR (400 MHz, CDCl₃) δ (ppm): 7.36 (s, 2H), 4.59 (d, J = 7.3 Hz, 2H), 2.25 (m, 2.32 – 2.19, 1H), 1.20 (m, 1.30 – 1.11, 32H), 0.80 (m, 6H). ¹³C NMR (101 MHz, CDCl₃) δ (ppm): 143.63, 129.41, 109.98, 61.13, 39.00, 31.86, 31.58, 31.55, 31.14, 29.74, 29.58, 29.42, 29.30, 29.21, 26.00, 22.64, 14.09.

2.2.6. Synthesis of 5,8-dibromo-2,3-di(thiophen-2-yl)quinoxaline

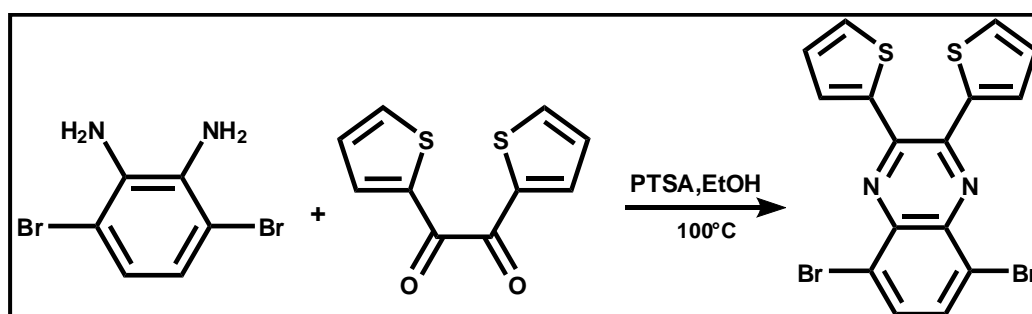


Figure 22. Synthesis of 5,8-dibromo-2,3-di(thiophen-2-yl)quinoxaline

3,6-Dibromobenzene-1,2-diamine (0.300 g, 1.12 mmol) and 2,2'-thienylglyoxal (0.251 g, 1.13 mmol) were dissolved in 30 mL ethanol and heated for 10-15 minutes before a catalytic amount of p-Toluenesulfonic acid (PTSA) was added. After addition of PTSA, product precipitated as a yellow solid at the base of reaction flux. Mixture was left for reflux at 100°C overnight. Then, precipitate was filtered and washed with EtOH until the yellow colour of solvent was disappeared. (0.42 g, 83%) ¹H NMR (400 MHz, CDCl₃), δ (ppm): 7.7 (s, 2H), 7.51 (7.56 – 7.46 (dd, 2H)), 7.42 (dd, 2H), 6.99 (s, 2H). ¹³C NMR (101 MHz, CDCl₃) δ (ppm): 146.95, 140.70, 138.44, 133.09, 130.42, 130.19, 127.70, 123.11.

2.2.7. Synthesis of 5,8-dibromo-2,3-diphenylquinoxaline

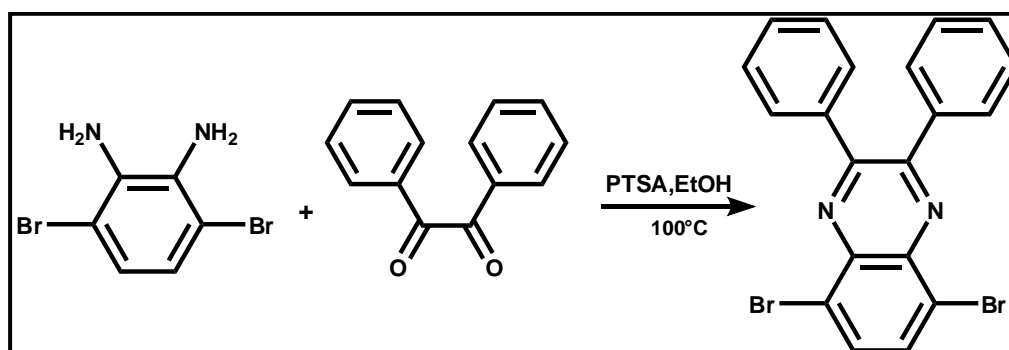


Figure 23. Synthesis of 5,8-dibromo-2,3-diphenylquinoxaline

3,6-Dibromobenzene-1,2-diamine (0.300 g, 1.128 mmol) and benzyl (0.237 g, 1.128 mmol) were dissolved in 30 mL of EtOH and heated for 10-15 minutes before catalytic amount of p-Toluenesulfonic acid (PTSA) were added. Mixture was left for reflux at 100°C overnight. Then, precipitate was filtered and washed with EtOH until the yellow colour of solvent was disappeared. (0.402g, 80% yield) ¹H NMR (400 MHz, CDCl₃), δ (ppm):7.85 (s, 2H), 7.59 (dd, 2H), 7.33 (7.42 – 7.25 (dd, 2H)). ¹³C NMR (101 MHz, CDCl₃) δ (ppm): 154.12, 138.85, 133.07, 130.23, 129.55, 128.35.

2.2.8. Synthesis of 10,13-dibromodibenzo[a,c]phenazine

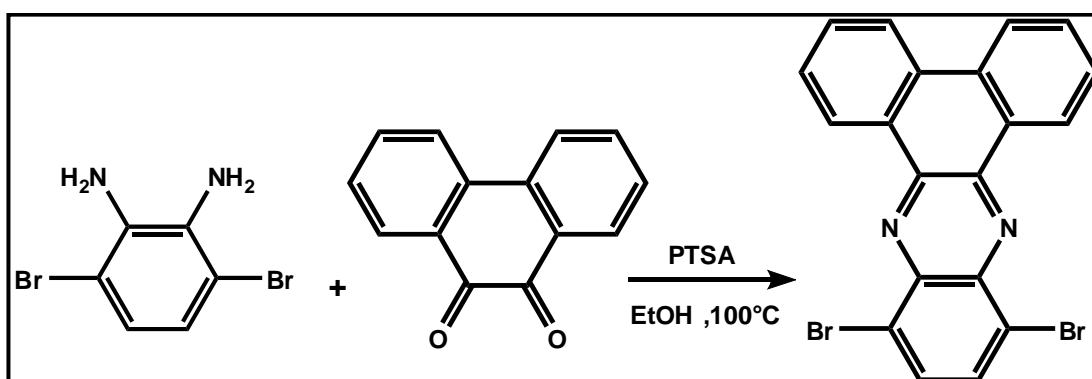


Figure 24. Synthesis of 10,13-dibromodibenzo[a,c]phenazine

3,6-Dibromobenzene-1,2-diamine (0.300 g, 1.128 mmol) and phenanthrene-9,10-dione (0.234 g, 1.128 mmol) were dissolved in 30 mL of EtOH and heated for 10-15 minutes before catalytic amount of p-Toluenesulfonic acid (PTSA) were added. Mixture was left for reflux at 100°C overnight. Then, precipitate was filtered and washed with EtOH until the yellow colour of solvent was disappeared. 10,13-dibromodibenzo[a,c]phenazine was obtained as a yellow powder.(0.326 g, 66% yield) ¹H NMR (400 MHz, CDCl₃) δ (ppm): 9.41 (d, J = 1.5 Hz, 2H), 8.50 (dd J = 1.5 Hz, 2H), 7.96 (s, 2H), 7.73 (7.80 – 7.67 (t, 4H)).

2.3. Synthesis of Polymers

2.3.1. Synthesis of P1

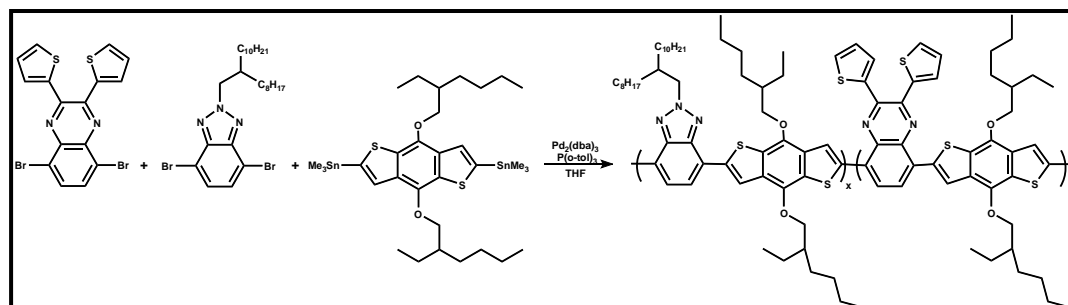


Figure 25. Synthesis of P1

For the synthesis of P1 Stille coupling reaction procedure was followed by putting together 4,7-dibromo-2-(2-octyldodecyl)-2H-benzotriazole (5) (0.246 g, 0.442 mmol) and 5,8-dibromo-2,3-di(thiophen-2-yl)quinoxaline (0.200 g, 0.442 mmol) and 2,6-Bis(trimethyltin)-4,8-bis(2-ethylhexyloxy)benzo[1,2-b:4,5-b']dithiophene (0.653g, 0.884mmol). After exposing monomer blend to argon gas, reactants were dissolved in 10 mL of dry tetrahydrofuran (THF) under argon atmosphere. Reaction solution was bubbled with argon for 40 minutes to remove air. After, catalytic amount of tris(dibenzylideneacetone)dipalladium(0) (0.0404g, 0.0442mmol) (5% of benzodithiophene unit) and tris(otolyl)phosphine (0.0269g, 0.0884) as a co-catalyst (10% of benzodithiophene unit) were added to the medium and reaction was refluxed at 70°C for 39 hours. Before addition of bromothiophene (0.216g, 1.327 mmol), catalyst tris(dibenzylideneacetone)dipalladium(0) (0.020g, 0.022 mmol) and co-catalyst tris(otolyl)phosphine (0.0135g, 0.0442mmol) were put into the solution and then reaction was stirred for 6 hours. After, trimethyl(thiophen-2-yl)stannane (0.990 g, 2.654 mmol) was added with same amount of extra catalyst that mentioned in previous sentences. Another 6 hours were spent before reaction was taken and cooled to the room temperature. Solvent was evaporated under reduced pressure and reaction was precipitated in cold methanol. After, solid residue was filtered by vacuum and purification was performed by Soxhlett apparatus.

Respectively, acetone, hexane and chloroform were spent to discard oligomers, small molecules, catalyst and other reactants. Polymer was collected by chloroform. After evaporation of solvent, polymer was precipitated in cold methanol again and vacuum filtration was used to obtain pure product.

GPC: Mn: 17.7 kDa, Mw: 35.0 kDa, PDI: 1.9

2.3.2. Synthesis of P2

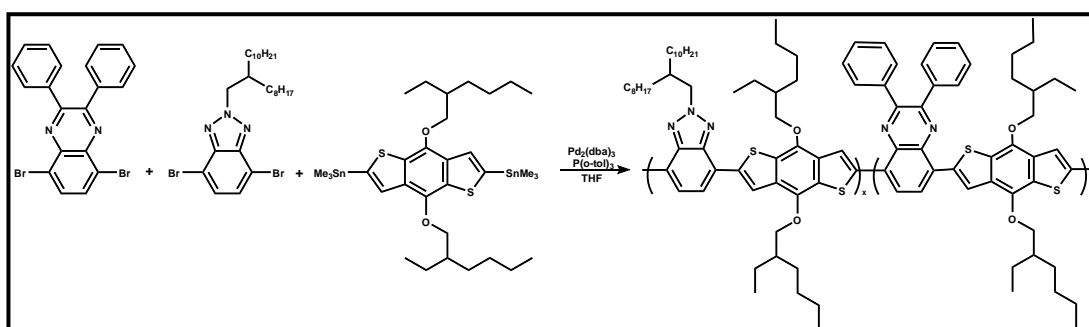


Figure 26. Synthesis of P2

Same procedure with P1 was pursued for the synthetic pathway of P2. Thus, 4,7-dibromo-2-(2-(octyldodecyl)-2H-benzo[d][1,2,3]triazole) (0.126 g, 0.227 mmol), 5,8-dibromo-2,3-diphenylquinoxaline (0.100 g, 0.227 mmol) and 2,6-Bis(trimethyltin)-4,8-bis(2-ethylhexyloxy)benzo[1,2-b:4,5-b']dithiophene (0.351 g, 0.454mmol) were mixed in reaction medium and kept under argon before addition of 8 mL of anhydrous tetrahydrofuran (THF). Reaction solution was bubbled with argon for 40 minutes to remove air. After, catalytic amount of tris(dibenzylideneacetone)dipalladium(0) (0.021g, 0.022mmol) and tris(otolyl)phosphine (0.014g, 0.045mmol) as a co-catalyst were added to the medium and reaction was refluxed at 70°C for 34 hours under argon atmosphere. Before addition of bromothiophene (0.111g, 0.682 mmol), catalytic amount of tris(dibenzylideneacetone)dipalladium(0) and co-catalyst tris(otolyl)phosphine were put into the solution. Then, reaction was stirred for 6 hours. After, trimethyl(thiophen-2-yl)stannane (0.508 g, 1,362 mmol) was added with extra catalyst. Another 6 hours were consumed before reaction was stopped and cooled to

the room temperature. Solvent was evaporated under reduced pressure and reaction was precipitated in cold methanol. After, solid residue was filtered by vacuum and purification was performed by Soxhlett apparatus. Polymer was collected by chloroform. After evaporation of solvent, residue was precipitated in cold methanol again and pure polymer was achieved by filtration.

GPC: Mn: 114.5 kDa, Mw: 743.9 kDa, PDI: 6.5

2.3.3. Synthesis of P3

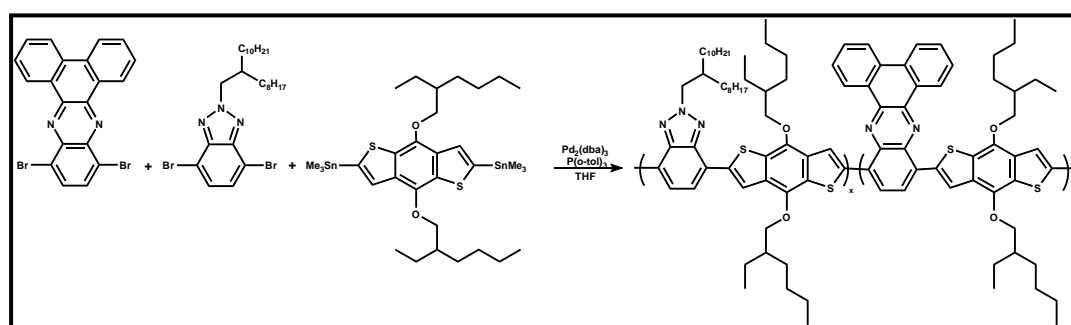


Figure 27. Synthesis of P3

Same procedure with P1 and P2 was applied for the synthetic pathway of P3. Thus, 4,7-dibromo-2-(2-octyldodecyl)-2H-benzo[d][1,2,3]triazole (0.127 g, 0.228 mmol), 10,13-dibromodibenzo[a,c]phenazine (0.100 g, 0.228 mmol) and 2,6-Bis(trimethyltin)-4,8-bis(2-ethylhexyloxy)benzo[1,2-b:4,5-b']dithiophene (0.352 g, 0.456 mmol) were mixed in reaction medium in 8 mL of anhydrous tetrahydrofuran (THF). Reaction solution was bubbled with argon for 40 minutes to remove air. After, catalytic amount of tris(dibenzylideneacetone)dipalladium(0) (0.021g, 0.022mmol) and tris(octyl)phosphine (0.014g, 0.045mmol) as a co-catalyst were added to the medium and reaction was refluxed at 70°C for 44 hours under argon atmosphere. Before addition of bromothiophene (0.111g, 0.682 mmol), catalytic amount of tris(dibenzylideneacetone)dipalladium(0) and co-catalyst tris(octyl)phosphine were put into the solution. Then, reaction was stirred for 6 hours. After, trimethyl(thiophen-2-yl)stannane (0.508 g, 1,362 mmol) was added with extra catalyst. Another 6 hours were consumed before reaction was stopped and

cooled to the room temperature. Solvent was evaporated under reduced pressure and reaction was precipitated in cold methanol. After, solid residue was filtered by vacuum and purification was performed by Soxhlett apparatus. Polymer was collected by chloroform. After evaporation of solvent, residue was precipitated in cold methanol again and pure polymer was achieved by filtration.

GPC: Mn: 14.0 kDa, Mw: 23.2 kDa, PDI: 1.7

2.4. Characterization of Conducting Polymers

2.4.1. Gel Permeation Chromatography

Gel permeation chromatography technique was used to investigate molecular weight and polydispersity index (PDI) of synthesized polymers. Working principle of the instrument is based on the segregation of macromolecules regarding to their hydrodynamic volumes. It contains solid stationary phase and liquid mobile phase. Calibration of device was performed by polystyrene standards.

2.4.2. Electrochemical Studies

Electrochemical studies were performed in order to examine p and n doping potentials and HOMO-LUMO levels of polymers. Electrochemical studies were conducted by using cyclic voltammetry (CV). The electrochemical reaction between polymers and stationary electrode with giving potential is the reason of the recorded data obtained from voltammogram. For measurement, firstly copolymers were dissolved in CHCl_3 and then spray coated on, indium tin oxide (ITO) coated glass. CV studies were carried out in three electrode systems. ITO, Pt wire and Ag wire calibrated to oxidation potential of Fc/Fc^+ redox couple serve as working electrode (WE), counter electrode (CE) and reference electrode (RE) correspondingly. Polymer coated ITO was submerged into 0.1 M tetrabutylammoniumhexafluorophosphate (TBAPF_6)/acetonitrile (ACN) solution used as supporting electrolyte. Gamry Instrument Reference 600 Potentiostat was utilized to record the redox reactions and

the color change of polymers with different potentials. At the end of the electrochemical studies, current density versus voltage diagram was plotted according to cyclic voltammetry studies.

2.4.3. Spectroelectrochemical Studies

Spectroelectrochemical studies include both spectroscopic and electrochemical measurements. These studies were utilized to investigate neutral state, polaron and bipolaron bands of copolymers and their optical changes with respect to applied potential. These studies have a place in proof of color change upon doping processes. In addition, optical band gaps (E_{gop}) of polymers and maximum absorption wavelengths (λ_{max}) were calculated from spectrometric studies. To that end, conductive polymers were coated on ITO glasses and put into TBAPF₆/ACN electrolyte solution in quartz cell. This system includes Ag/Ag⁺ as reference electrode and Pt wire as counter electrode. Oxidation of polymers was achieved upon applied potential and absorption spectra were recorded concurrently.

2.4.4. Kinetic Studies

Kinetic studies were done to examine the switching time and optical contrast values of polymers between natural and oxidation state. Studies were performed by exposing polymer covered ITO glass to square wave potential with 5 s time intervals in 0.1 M TBAPF₆/ACN. Percent transmittance differences between two states of polymers and also the time required to switch between two states were examined in Vis and NIR regions of the spectra. As a result, percent transmittance change (%T) versus time graph was obtained and the switching times were calculated with respect to this graph.

2.4.5. Thermal Studies

For thermal analyses, thermal gravimetric analysis (TGA) and differential scanning calorimetry (DSC) techniques were performed. TGA were utilized for the investigation of weight losses upon temperature. Also, TGA gives information about the decomposition temperatures of polymers. For this purpose, Perkin Elmer Pyris 1 Thermal Gravimetry Analysis was used. On the other hand, DSC studies were performed to give information about crystalline and amorphous structure of synthesized polymers. Glass transition temperatures (T_g) and melting points (T_m) of polymers can be obtained from this thermal study. Perkin Elmer Differential Scanning Calorimetry was used for DSC studies.

2.4.6. Photovoltaic Studies

Photovoltaic studies include the construction of a solar cell device and the measurement of efficiencies under illumination. A BHJ polymer solar cell includes the layers of ITO, PEDOT: PSS, Polymer: PC₇₁BM, LiF and Al. ITO glass substrate that purchased from Visiontek Systems was partially etched by using HCl-HNO₃ solution and cleaned with toluene, Hellmanex as detergent, water and isopropyl alcohol in ultrasonic bath for 15 min respectively. After the desiccation with N₂, oxygen plasma cleaning step was done with using Harrick Plasma Cleaner to remove residue organic impurities on ITO. Then, filtered PEDOT-PSS solution was coated on clean ITO surface by using spin coating technique. Substrate was exposed to 150°C temperature for 15 min to remove residual water. Polymer- PC₇₀BM blends with different weight ratios were prepared and coated with using spin coating technique in the N₂ filled glove-box system. (O₂ concentration < 1 ppm and H₂O concentration < 1 ppm). LiF and Al were thermally evaporated by using vacuum. Keithley 2400 source meter was used to record current-voltage characteristic (J-V) curves under AM 1.5 G illuminations via Atlas Material Testing Solutions solar test 1200 solar simulator.

CHAPTER 3

RESULTS AND DISCUSSION

3.1. Optical Studies

UV-Vis spectra of all three polymers in both thin film and chloroform solution are illustrated in Figure 28 and results are summarized in Table 1. P1, P2 and P3 demonstrated broad visible light absorption as expected. Copolymers P1, P2 and P3 showed two absorption maxima that includes one in a short wavelength zone due to $\pi-\pi^*$ transition of conjugated polymer backbone and the other in long wavelength zone due to intramolecular charge transfer from donor to acceptor units.¹⁰² Maximum absorption values of P1, P2 and P3 in thin film were recorded as 374/539, 493/535 and 488/532 nm respectively. Also, λ_{\max} values of P1, P2 and P3 in CHCl_3 solution were observed as 369/530, 491/534, 486/529 nm correspondingly.

Table 1. Summary of the optical studies of P1, P2 and P3 in chloroform solution and thin film form

	Solution λ_{\max} (nm)	Thin Film λ_{\max} (nm)
P1	530	539
P2	534	535
P3	529	532

The maximum absorption peaks of P1, P2 and P3 in thin film were nearly identical to peaks in solution state that were red shifted by only 9, 1 and 3 nm respectively. Intermolecular stacking and conformational alterations causes to shift of the spectra for polymers.¹⁰³ Red shift in thin film form can be explained by decrease in conformational freedom, aggregation or due to interaction between solvent and

polymer chains.¹⁰⁴ Such a low differences between thin film and solution state attests the shortage of aggregation and weak solvent-polymer interaction. Apparently, polymers made reunion in thin film state and showed pre-aggregates in solution because of the strong inter chain interactions.¹⁰⁵ Despite the fact that low red shift behaviour was observed for polymers, P3 was expected to show highest red shift value among them due to its fused structure and high planarity. However, highest red shift could not be achieved by P3 that could be because of the low molecular weight of polymer while comparing with other polymers.

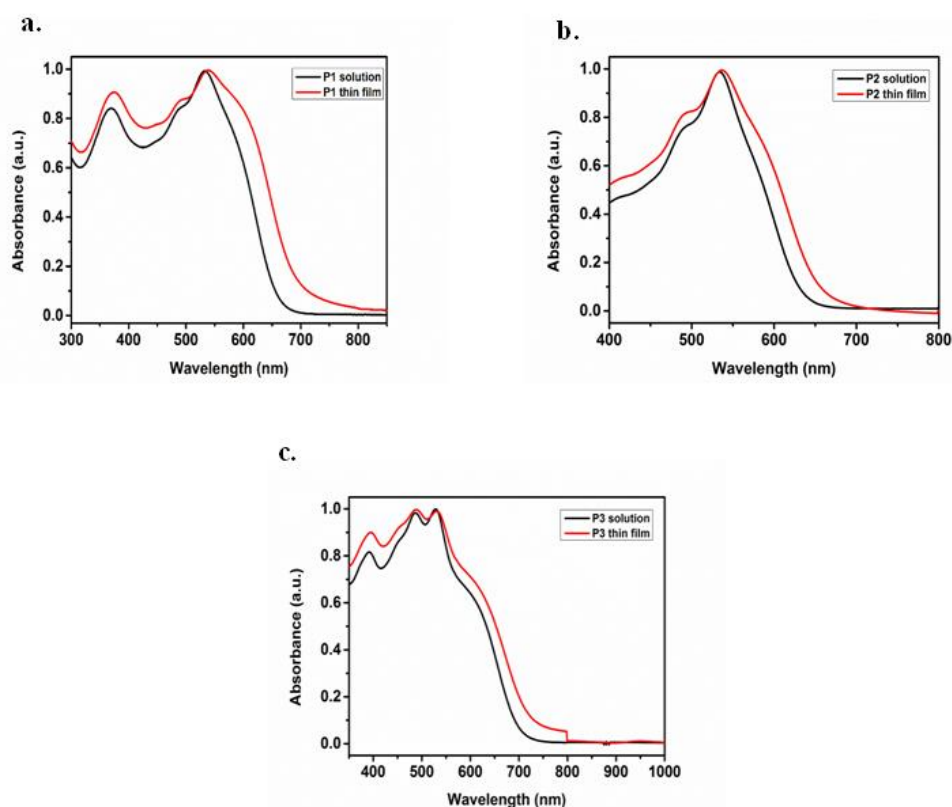


Figure 28. Absorption spectra of P1, P2 and P3 in chloroform solution and thin film form

3.2. Electrochemical Studies

Cyclic voltammetry (CV) studies were performed to examine redox potentials and HOMO-LUMO energy levels of three random polymers. For measurement, copolymers were dissolved in CHCl_3 (5mg/mL) and spray coated on ITO coated glass surface. CV studies were carried out in three electrode system including ITO as a working electrode, Pt wire as a counter electrode, Ag wire as a reference electrode in 0.1 M tetrabutylammoniumhexafluorophosphate (TBAPF_6)/acetonitrile (ACN) solution as supporting electrolyte. Recorded electrochemical data of all polymers were obtained from cyclic voltammograms as indicated in Fig. 29 and summarized in Table 2. All polymers have ambipolar doping character as shown in Fig. 29. Oxidation potential (p-doping) of P1 was recorded at 1.10 V with a dedoping peak at 0.32V. Oxidation potential of P2 was observed at 1.08 V with a dedoping potential of 0.73V. Finally, oxidation potential of P3 was 1.00 V with a couple at 0.50 V. N-type doping, potentials of P1, P2, and P3 were recorded at -1.50V/-1.95V, -1.43V/-1.93V and -1.48V/-1.91V respectively. Dedoping potentials of polymers were found as 1.28V/-1.50V, -1.36V/-1.53V, -1.15V/-1.52V in return. When comparing all three polymers in terms of their oxidation-reduction potentials as expected P3 was demonstrated lower oxidation potential due to high electron density of its fused phenyl structure when comparing with P2. Although thiophene unit has more electron donating ability and P1 is expected to perform oxidation and reduction processes easier than benzene substituted P2, oxidation potential of P1 is nearly same with P2 yet more. This result can be attributed to the low conjugation length of P1 when compared with its counterpart.

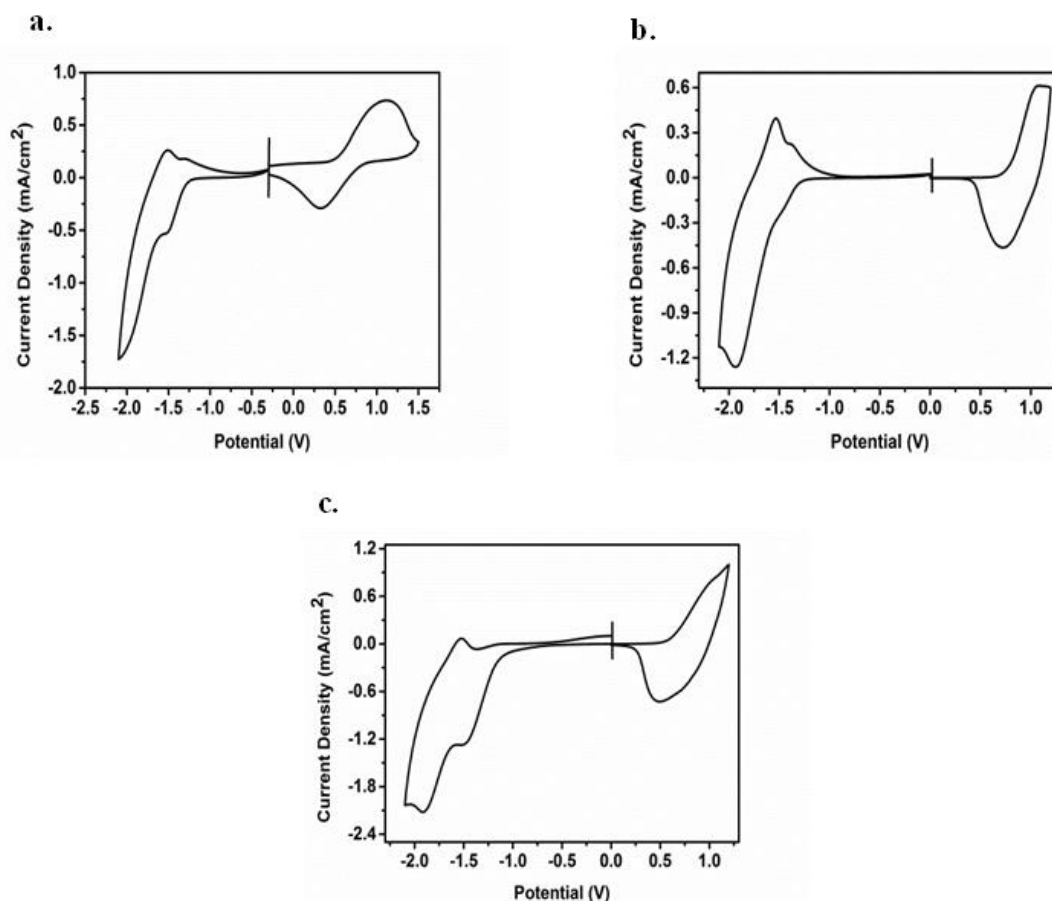


Figure 29. Single-scan cyclic voltammograms of polymer films in 0.1 M TBAPF₆/ACN electrolyte solution a) P1 b) P2 c) P3

HOMO and LUMO energy levels were estimated by taking normal hydrogen electrode value as -4.75 eV. HOMO-LUMO energy levels were calculated by following equations:

$$\text{HOMO} = - (4.75 + E_{\text{ox}}^{\text{onset}})$$

$$\text{LUMO} = - (4.75 + E_{\text{red}}^{\text{onset}})$$

HOMO energy levels of random copolymers were calculated as -5.15 eV, -5.52 eV and -5.35 eV for P1, P2 and P3 correspondingly. HOMO energy levels are crucial parameters for solar cell applications. To achieve a successful hole transfer in solar cell application, HOMO level of the donor unit should be higher than that of

acceptor. All polymers show higher HOMO levels when compared with that of PCBM which has a -6.10 eV HOMO energy level.¹⁰⁶ As seen, P1 shows the highest lying HOMO level that may affect the power conversion efficiency value negatively with lowering V_{OC} value. With the replacement of thiophene substituent by benzene, lower HOMO level than P1 was obtained from P2. P2 demonstrates the lowest HOMO level which can provide high V_{OC} and good air stability during the photovoltaic applications. Also, LUMO level of the polymer is another crucial criterion for polymers in order to perform a good charge separation. For an effective charge separation, energy difference between LUMO level of donor unit and LUMO level of acceptor should be larger than 0.3 eV.¹⁰⁷ According to CV studies, LUMO levels of polymers were found as -3.45, -3.47 and 3.63 eV for P1, P2 and P3. LUMO level of acceptor PC₇₁BM is -4.2 eV and according to results P3 could demonstrate more effective charge separation than P1 and P2.

Electronic band gap of random copolymers was calculated according to the following equation:

$$E_g^{el} = \text{HOMO} - \text{LUMO}$$

From the equation, electronic band gap of P1, P2 and P3 were calculated as 1.70, 2.05, and 1.72 eV, respectively. It is a common result that E_g^{el} of a conjugated polymer is greater than E_g^{op} because charge species such as polarons can locate on polymer chain and some energy barriers can occur at electrodes during charge transfer. Although P2 and P3 follow this usual trend, P1 demonstrates higher optical band gap value compared with its electronic band gap. Such an unusual result can be explained by uncompleted oxidation of the polymer during doping procedure by cyclic voltammetry. P3 shows lower electronic band gap than P2 due to fused phenyl ring structure that enhances both planarity and conjugation length and also makes easier the electron transportation with its two connected benzene rings. P1 bearing thiophene based quinoxaline unit has lower band gap than P2. Band gap of a polymer is decreased with the quinoid resonance stabilization.³ Thiophene unit can generate

quinoid form easier than the benzene ring due to the low aromatic resonance stabilization which resulted with low band gap of P1.¹⁰⁸

The differences between HOMO, LUMO and electronic band gap values of polymers are mainly because of the change in electron density and donating abilities of side groups. It can be concluded that conjugated substituent groups certainly affect the electronic properties of the polymers.

Table 2. Electrochemical Properties of P1, P2 and P3

	$E_{p-doping}$ (V)	$E_{p-dedoping}$ (V)	$E_{n-doping}$ (V)	$E_{n-dedoping}$ (V)	HOMO (eV)	LUMO (eV)	E_g^{el} (eV)
P1	1.10	0.32	-1.50/ -1.95	-1.28/ -1.50	-5.15	-3.45	1.70
P2	1.08	0.73	-1.43/ -1.93	-1.36/ -1.53	-5.52	-3.47	2.05
P3	1.00	0.50	-1.48/ -1.91	-1.15/ -1.52	-5.35	-3.63	1.72

3.3. Spectroelectrochemical Studies

For spectroelectrochemical studies, after coating the conductive polymers on ITO glasses, external potential was applied to the polymer film stepwise and spectra are obtained from UV–Vis–NIR spectroscopy as illustrated in Fig. 3. Potential was applied between 0.0 V and 1.2 V for P1 and P2, 0.0 V and 1.1 V for P3 steadily. In order to obtain accurate neutral state absorption, polymer thin films were exposed to constant potential to remove any trapped charge or ion before the measurements.

Dual maximum absorption wavelengths were recorded for all polymers at 374/539, 493/535 and 488/532 for P1, P2 and P3 respectively. During the p type doping process, while the absorption in visible zone started to reduce due to the formation of polaron and bipolaron which are the charge carriers on polymer chain, new absorption bands at high wavelengths arouse. Although absorption at low energy regions should increase with increasing potential and formation of bipolarons, for all P1, P2 and P3 absorption in near IR region could not achieved the increment and absorption in bipolaron region could not be higher than polaron region as shown in Fig. 30. This result could be because of the prevention of further oxidation during the measurement.

Optical band gap (E_g^{op}) values of P1, P2 and P3 were calculated from the onsets of lowest π - π^* transitions according to $E_g^{op} = 1241/\lambda_{onset}$ and found as 1.74 eV, 1.87 eV and 1.70 eV correspondingly as illustrated in Table 3. Optical band gap value of P1 is smaller than that of P2. For P2, substituted benzene rings on quinoxaline moiety have the ability of rotation, which interrupts the packing and enhance charge carrier mobility. It is worthy of note that introduction of thiophene ring to the quinoxaline unit instead of benzene ring, elongates the conjugation length. In addition, because electron donating ability of thiophene is higher than benzene, higher HOMO level was obtained for P1. Relatively low band gap of thiophene based polymer provide opportunity to make high absorption at high wavelength region of solar spectrum.⁹³ Aim of having a broad visible absorption was successfully achieved by spinning red, blue and green region of spectrum on polymer backbone.

Table 3. Spectroelectrochemical results of P1, P2 and P3

	λ_{max} (nm)	E_g^{op} (eV)
P1	374/539	1.74
P2	493/535	1.87
P3	488/532	1.70

On the other hand, the donor group on polymer backbone affects the absorption spectra, band gap value and all optical properties of polymers. In literature, random copolymer of CoP1, CoP2 and CoP3 published by our group, including thiophene unit as donor and same quinoxaline and benzotriazole units as acceptor demonstrate lower optical band gap values while comparing with P1, P2 and P3.⁹⁷ Benzodithiophene unit has more electron donor character with its benzene fused thiophene structure and also offers longer conjugation length thus polymer synthesized in this study are expected to show lower band gap when comparing with CoP1, CoP2 and CoP3. The underlying reason behind this unexpected result can be the stronger π stacking ability of small thiophene unit, that reduces steric hindrance and enhance interchain π - π stacking for effective charge carrier mobility.¹⁰⁹ Also, because of the differences during the polymerization processes, P1, P2 and P3 could have lower solubility than their counterparts and low solubility of polymers could cause low conjugation length that results with lower band gaps.

For the scientific expression of colors, colorimetric measurements of the thin film state polymers were performed at all stages of the oxidation process and color of polymers were identified with using CIE (Commission Internationale de l'Eclairage) coordinates. CIE coordinate system composes of three components including luminance (L), hue (a), and saturation (b). Colors of natural and oxidized-reduced state of polymers are demonstrated in Fig. 30 and colorimetric studies results including L,a,b values of are summarized in Table 4.

Table 4. L,a,b values of P1, P2 and P3

P1	-2.1 V	0.0 V	1.1 V	1.2 V
l	47	20	22	26
a	-4	6	3	3
b	0	-3	5	5

P2	-2.0 V	0.0 V	1.0 V	1.2 V
l	47	21	40	44
a	-4	6	5	2
b	-3	-3	-1	0

P3	-2.1 V	0.0 V	0.9 V	1.1 V
l	51	12	17	23
a	-5	6	4	4
b	2	2	5	2

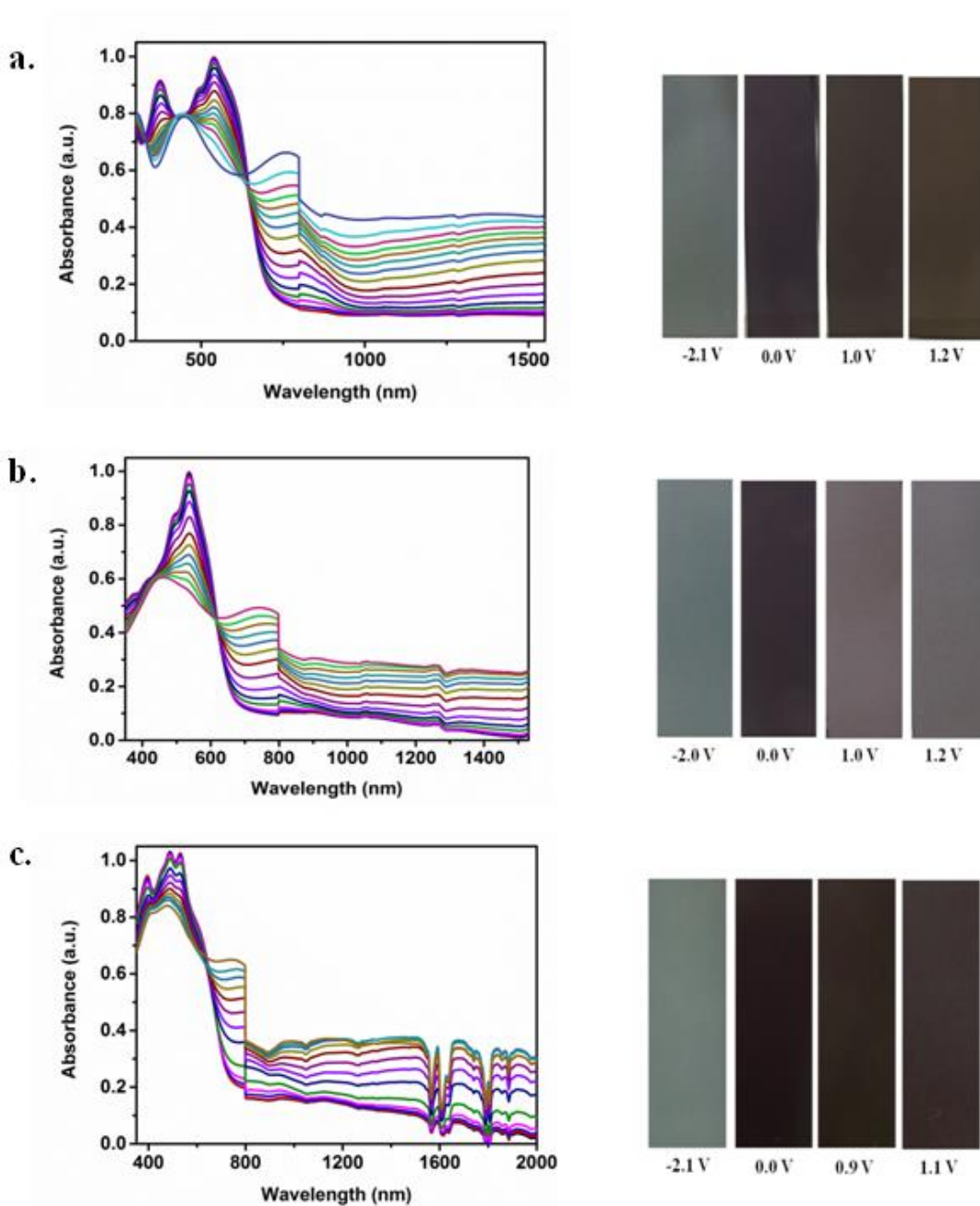


Figure 30. UV-Vis-NIR spectra and colors at different potentials of a) P1 , b) P2 and c) P3 in 0.1 M TBAPF₆/ACN electrolyte solution

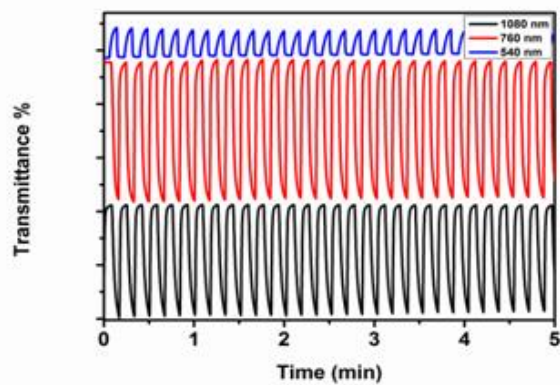
3.4. Kinetic Studies

Kinetic studies were performed in order to investigate switching time and optical contrast between two extreme states of copolymers. Optical contrast basically is the percent transmittance change at a given wavelength and switching time is the time required switch between neutral and oxidized states. For kinetic studies, polymer coated ITO glass was exposed to sweeping potential between two states with 5 s time intervals in 0.1 M TBAPF₆/ACN solution with respect to their doped and de-doped states. As illustrated in Table 5, optical contrast values were found as 11% at 540 nm, 52% at 760 nm and 43% at 1080 nm for P1 with switching times of 1.3, 1.4 and 1.7 s correspondingly. P2 demonstrated 31% at 536 nm, 42% at 750 nm and 35% at 1470 nm optical contrast values and switching times were recorded as 2.4, 1.2, 0.9 s. Optical contrast values for P3 were examined as 13% at 545 nm, 53% at 760 nm and 51% at 1700 nm with switching times of 2.9, 1.1 and 0.7 s respectively.

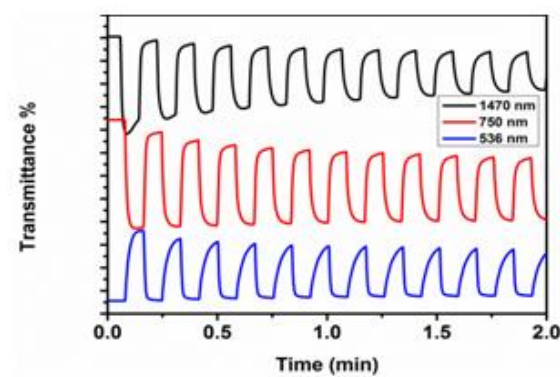
Table 5. Optical contrast and switching time values of P1, P2 and P3

	Optical Contrast		Switching Times
	(ΔT %)		(s)
	43	1080 nm	1.7
P1	52	760 nm	1.4
	11	540 nm	1.3
	35	1470 nm	0.9
P2	42	750 nm	1.2
	31	536 nm	2.4
	51	1700 nm	0.7
P3	53	760 nm	1.1
	13	534 nm	2.9

a.



b.



c.

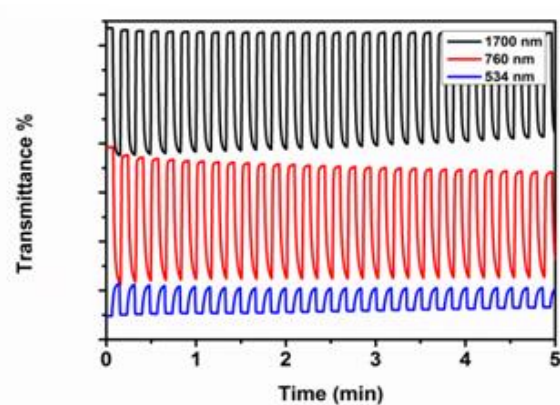


Figure 31. Percent transmittance change of a) P1 b) P2 c) P3 in 0.1 M TBAPF₆ / ACN electrolyte solution at given wavelengths

3.5. Thermal Studies

Thermal studies include the TGA and DSC studies of the polymers. Analyses were achieved under nitrogen atmosphere. All TGA measurements were made with heating rate of 10°C/min between 30°C and 600°C. TGA results demonstrate that for P1, P2 and P3 43.58%, 46.05% and 45.36% mass losses were observed at 315°C, 295°C and 300°C, respectively. DSC studies were performed with heating rate of 10°C/min between 20°C and 300°C. According to obtained curves, P1; P2 and P3 did not demonstrate glass-transition temperature (T_g). This could be attributed to the rigid structures of synthesized polymers. TGA and DSC analysis results were given in Appendix A.

3.6. Photovoltaic Studies

Electrochemical studies prove that polymers have suitable band gap values and HOMO-LUMO energy levels for solar cell application that arrange with the energy levels of other materials utilized in solar cell application as given in Fig. 32.

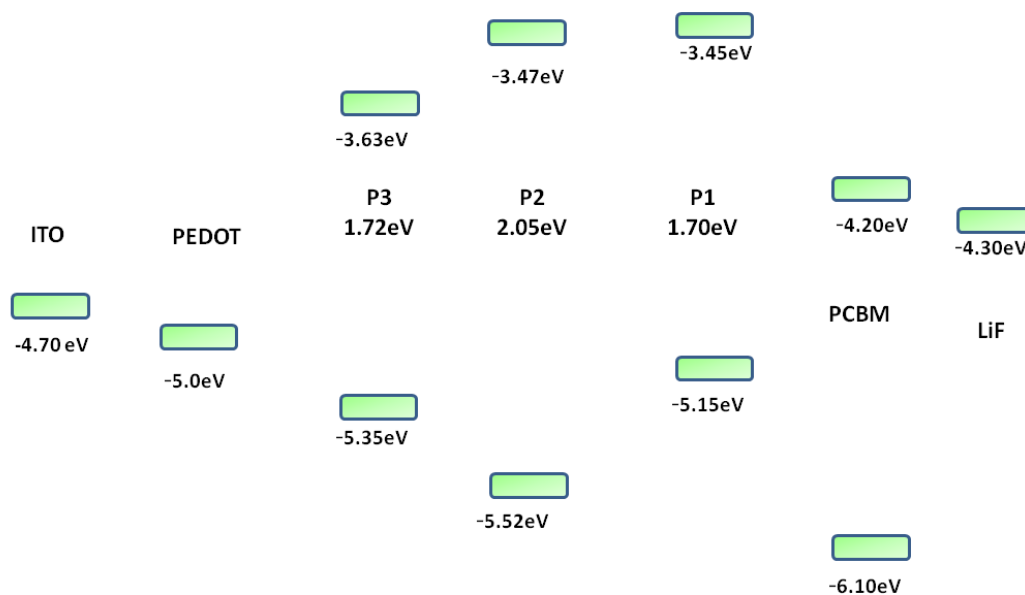


Figure 32. Energy levels of materials utilized in organic solar cell device construction

Construction of organic solar cell devices were performed with the typical configuration of ITO/PEDOT:PSS/Polymer:PC₇₁BM/LiF/Al correspondingly. Construction of all layers are important to achieve a solar cell with high PCE. PC₇₁BM was chosen as the acceptor material in active layer due to its wider and stronger absorption ability while comparing with other fullerene derivatives that improves the current passes through the solar cell and enhance the PCE.¹¹⁰ In addition, polymer: PCBM ratio is the one of the crucial parameter that plays important role on efficiency. Transportation of electrons enhances with increasing PC₇₁BM amount in active layer that result with the high short circuit current value and PCE. However, high PCBM ratio brings with low polymer amount in active layer that causes to decrease in collected photons and short circuit current ultimately. Therefore, amounts of polymer and PCBM should be optimized to obtain high PCE. For the determination of optimum composition, organic solar cells were constructed by applying polymer: PCBM blends with different ratios on PEDOT:PSS coated ITO surface by spin coating technique. Then, LiF and Al were thermally evaporated on these layers. Then, current density-voltage characteristic of the devices were observed under illumination of AM 1.5 G with 100 mW/cm². Current density-voltage curve of devices with P1, P2 and P3 are given in Figure 33, 34 and 35.

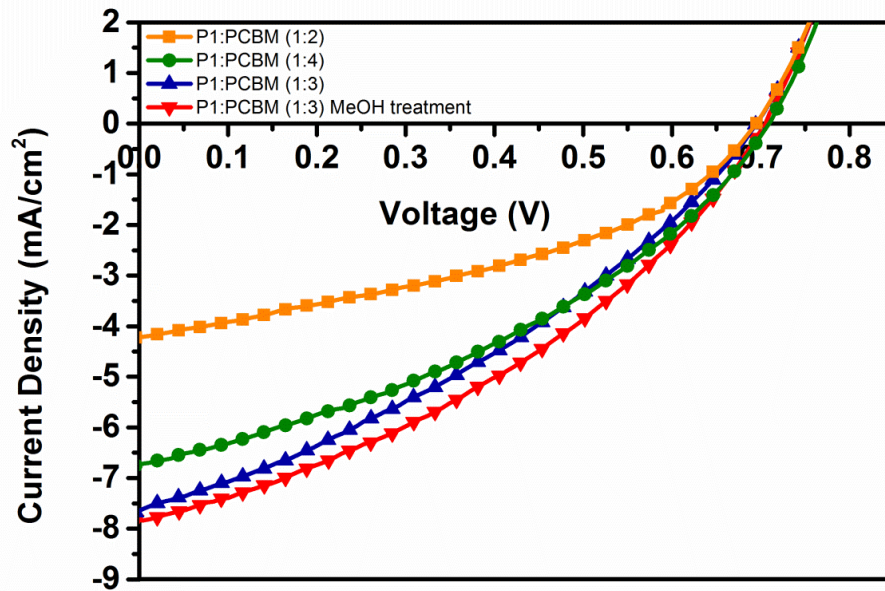


Figure 33. Current density-voltage curve of devices with P1

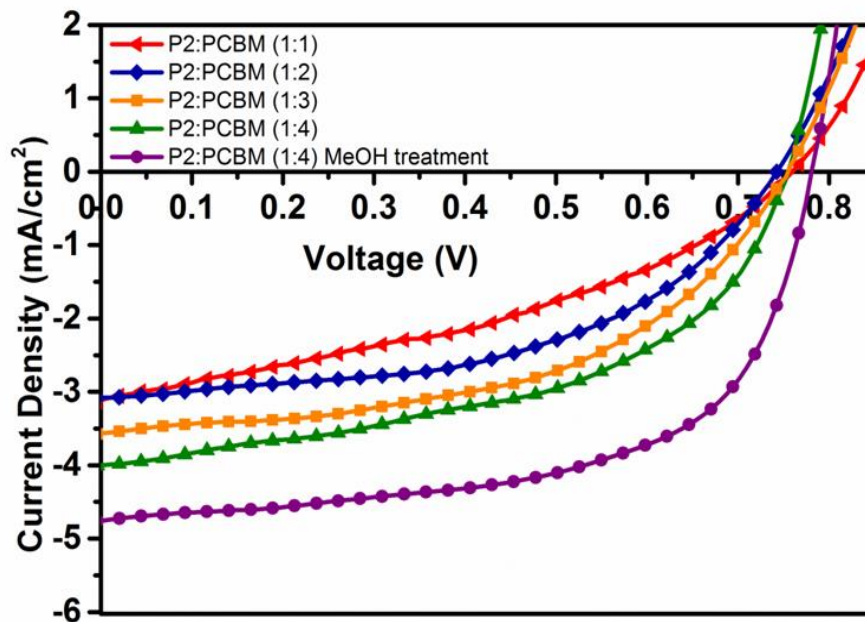


Figure 34. Current density-voltage curve of devices with P2

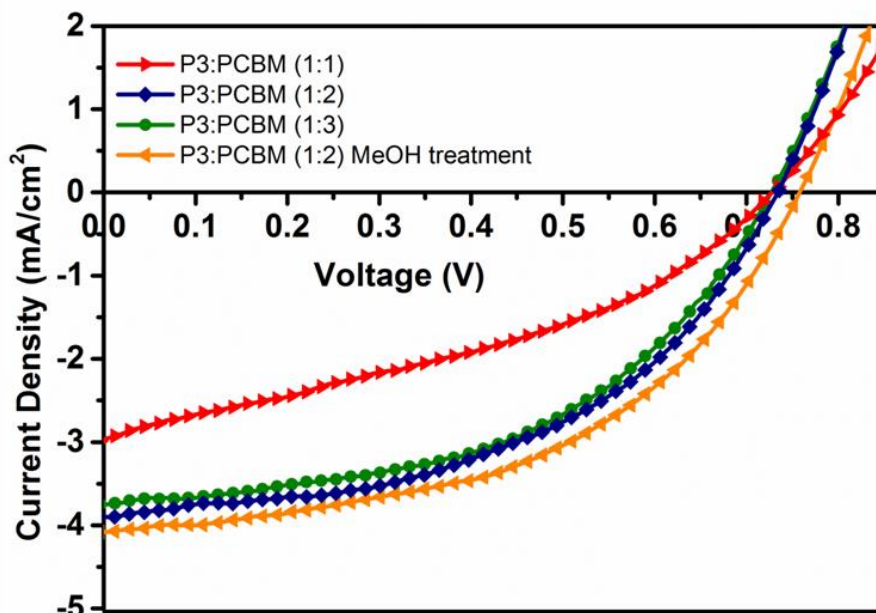


Figure 35. Current density-voltage curve of devices with P3

From their I-V graphs all important parameters including V_{OC} , J_{sc} , FF were estimated, and power conversion efficiency values were calculated for all devices depending on composition. Among them, P2 demonstrates best solar cell efficiency as 2.22%. Although P2 has highest band gap value among them, its photovoltaic device has highest PCE value of 2.22% which could be thanks to the high molecular weight that enhances intermolecular charge hopping process by increasing polymer chain length.¹¹¹ This phenomenon could also be the reason of the low PCE of P3 which has lower molecular weight while comparing with P1 and P2. For all polymers, best device performance values were recorded in *o*-dcb solution. Also, for all polymers, device performances were enhanced by applying MeOH treatment by raising both V_{OC} and J_{sc} values. The reason behind this increment is because of the optimization of the phase separation and improvement of the interface between active layer and PEDOT:PSS.¹¹²

For P1, best PCE result was calculated as 2.03 % for P1: PC₇₁BM (1:3, w:w) with V_{OC} values of 0.70 V and J_{SC} values of 7.85 mA/cm². Fill factor value for the best device is 37% for P1. P1 demonstrates high J_{SC} value between 4.22-7.85 mA/cm² that could be due to high absorption ability of the polymer. For P2, best PCE result was obtained as 2.22% from the device of P2:PC₇₁BM (1:4, w:w) with MeOH treatment. V_{OC} value is 0.78 V, J_{SC} is 4.74 mA /cm² and FF is 60% for this device configuration. Finally, for P3 highest device performance was recorded by P3: PC₇₁BM (1:3, w:w) ratio with MeOH treatment as 1.52%. V_{OC}, J_{SC} and FF values were estimated as 0.76V, 4.08 mA /cm² and 49%, respectively.

Table 6. Summary of the photovoltaic studies of P1

P1:PCBM (w:w)	V_{OC} (V)	J_{SC} (mA/cm²)	V_{MP} (V)	J_{MP} (mA/cm²)	FF (%)	PCE (%)	Treatment
(1:2)	0.69	4.22	0.47	2.49	40	1.16	-
(1:3)	0.69	7.68	0.41	4.39	34	1.80	-
(1:3)	0.70	7.85	0.43	4.72	37	2.03	MeOH
(1:4)	0.71	6.74	0.41	4.23	36	1.72	-

Table 7. Summary of the photovoltaic studies of P2

P2:PCBM (w:w)	V_{OC} (V)	J_{SC} (mA/cm²)	V_{MP} (V)	J_{MP} (mA/cm²)	FF (%)	PCE (%)	Treatment
(1:1)	0.76	3.08	0.47	1.92	38	0.89	-
(1:2)	0.74	3.09	0.52	2.21	50	1.15	-
(1:3)	0.75	3.56	0.52	2.63	51	1.36	-
(1:4)	0.75	4.00	0.55	2.72	50	1.49	-
(1:4)	0.78	4.74	0.62	3.61	60	2.22	MeOH

Table 8. Summary of the photovoltaic studies of P3

P3:PCBM (w:w)	V _{OC} (V)	J _{SC} (mA/cm ²)	V _{MP} (V)	J _{MP} (mA/cm ²)	FF (%)	PCE (%)	Treatment
(1:1)	0.73	2.97	0.48	1.67	37	0.80	-
(1:2)	0.73	3.90	0.49	2.80	48	1.37	-
(1:3)	0.73	3.73	0.49	2.71	49	1.33	-
(1:2)	0.76	4.08	0.51	2.99	49	1.52	MeOH

Incident photon to current efficiency (IPCE) method was performed in order to estimate the ratio of number of charges stored in electrodes to the number of incident photons. IPCE values were recorded by scanning the range between 300-900 nm. For measurement, best solar cell devices with MeOH treatment were prepared by 1:3, 1:4 and 1:2 (w:w) polymer:PC₇₁BM ratio for P1, P2 and P3 respectively. Maximum IPCE values were recorded as 43.72% for P1, 21.60% for P2 and 19.51% for P3 and shown in Fig. 36.

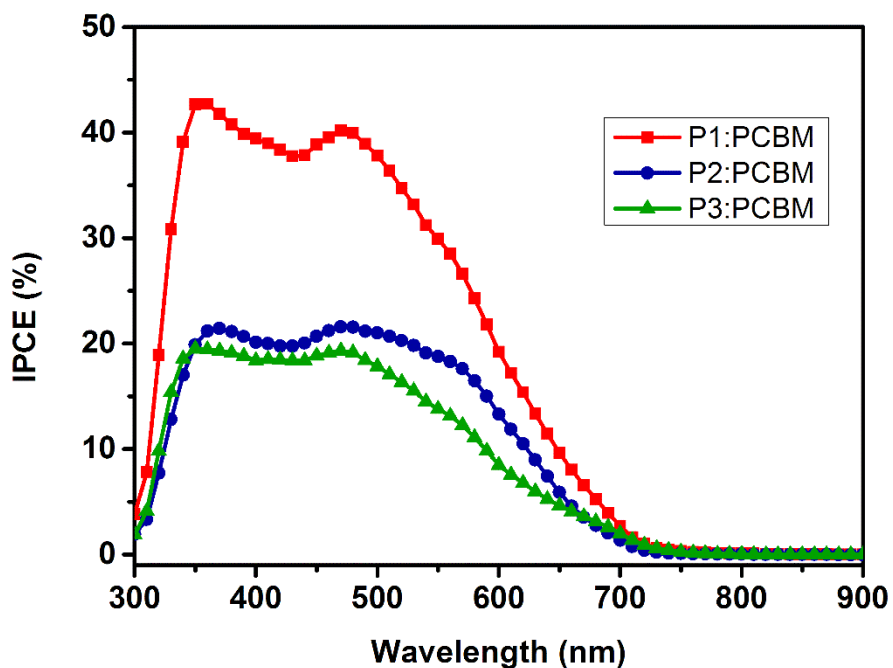


Figure 36. IPCE curves of best performance solar cells of P1, P2 and P3

3.7. Morphology

Atomic force microscopy (AFM) and transmission electron microscopy (TEM) were utilized in order to get information on the morphology of the devices. For this purpose, AFM and TEM analyses of active layers showing the best performance were conducted and the images are shown in Fig. 7. The root mean square roughness (R_{ms}) of the active layers was measured from the active layers of P1:PC₇₁BM (1: 3, w: w), P2 : PC₇₁BM (1:4, w:w) and P3:PC₇₁BM (1:2, w:w) as 1.54 nm, 5.42 nm and 2.15 nm, respectively. Also, the thicknesses of the best performance active layers were estimated as 138 nm for P1: PC₇₁BM (1:3, w:w), 123 nm for P2 : PC₇₁BM (1:4, w:w) and 124 nm for P3 : PC₇₁BM (1:2, w:w). The darker areas in the TEM images correspond to the PCBM rich areas while the lighter ones are the contributions of the polymer rich areas.

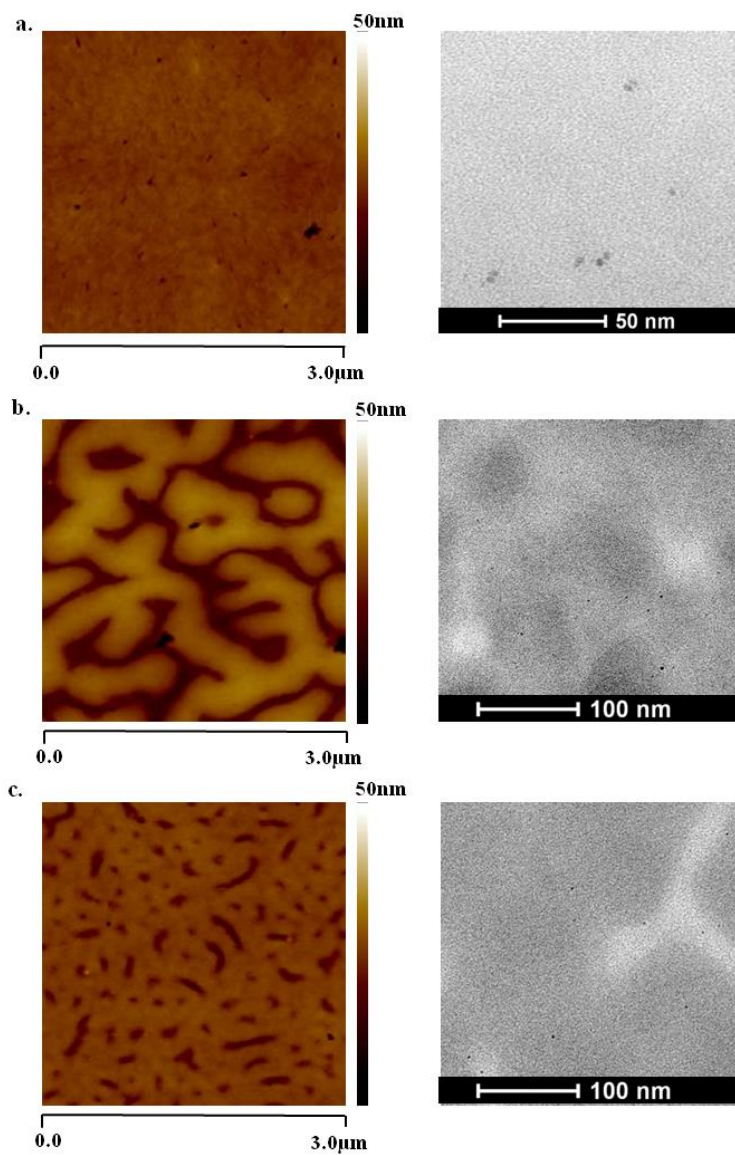


Figure 37. AFM and TEM Images of a) P1:PC71BM (1:3) and b) P2:PC71BM (1:4) and a) P1:PC71BM (1:2)

CHAPTER 4

CONCLUSIONS

In this study, quinoxaline, benzotriazole and benzodithiophene bearing random copolymers were successfully synthesized by following Stille coupling reaction procedure for photovoltaic application. This study aimed to produce polymers with broad visible light absorption by combining benzodithiophene and quinoxaline moieties on polymer backbone, which demonstrates maximum absorption value around 600-730 nm in literature, and also benzotriazole and benzodithiophene units that show maximum light absorption at around 500 nm in literature. Broad visible light absorption was achieved for P1, P2 and P3 that demonstrate maximum absorption peaks at 374/539, 493/535 and 488/532 nm respectively. Optical band gap values of the polymers were calculated from the onsets of lowest π - π^* transitions as 1.74 eV, 1.87 eV and 1.70 eV for P1, P2 and P3. Optical contrast values of the P1 were recorded as 11% (540 nm), 52% (760 nm) and 43% (1080 nm) with switching time values of 1.3, 1.4 and 1.7 seconds respectively. Optical contrast values of P2 are 31% (536 nm), 42% (750 nm) and 35% (1470 nm) and switching times of P2 were estimated as 2.4, 1.2 and 0.9 seconds in return. P3 achieved 51% optical contrast value at 1700 nm with 0.7 s switching time, 53% at 760 nm with 1.1 s and 13% at 534 nm with 2.9 s. From the electrochemical studies, HOMO energy levels of the polymers were calculated as -5.15, -5.52 and -5.35 eV while their LUMO levels were -3.45, -3.47 and 3.63 eV respectively. From HOMO-LUMO energy levels electronic band gaps were calculated as 1.70, 2.05, and 1.72 eV for P1, P2 and P3. All these values and calculations prove that three random copolymers could be definitely utilized as donor material in the active layer of solar cell application with their HOMO-LUMO energy levels and band gaps.

In the light of these information, bulk heterojunction type solar cells were successfully constructed with a device structure of ITO/PEDOT:PSS/Polymer:PC₇₁BM/LiF/Al and their investigations were made to obtain current density-voltage characteristics of devices under AM 1.5G illumination. Thanks to the broad visible light absorption character of the copolymers, best results were recorded as 2.03 % for P1 with P1: PC₇₁BM (1:3, w:w) ratio, 2.22% from the device of P2:PC₇₁BM (1:4, w:w) ratio and 1.52% for P3 with P3: PC₇₁BM (1:2, w:w) ratio.

REFERENCES

- (1) Chiang, C. K.; Fincher, C. R.; Park, Y. W.; Heeger, A. J.; Shirakawa, H.; Louis, E. J.; Gau, S. C.; MacDiarmid, A. G. *Phys. Rev. Lett.* **1977**, *39* (17), 1098–1101.
- (2) Rahman, M. A.; Kumar, P.; Park, D.-S.; Shim, Y.-B. *Sensors* **2008**, *8* (1), 118–141.
- (3) Coakley, K. M.; McGehee, M. D. *Chemistry of Materials*. **2004**, *16* (23), 4533–4542
- (4) Ye, H.; Zhao, B.; Li, D.; Chen, D.; Xie, G.; Su, S. J.; Yang, W.; Cao, Y. *Synth. Met.* **2015**, *205*, 228–235.
- (5) Bolognesi, M.; Gedefaw, D.; Dang, D.; Henriksson, P.; Zhuang, W.; Tessarolo, M.; Wang, E.; Muccini, M.; Seri, M.; Andersson, M. R. *RSC Adv.* **2013**, *3* (46), 24543.
- (6) Turan, J.; Kesik, M.; Soylemez, S.; Goker, S.; Coskun, S.; Unalan, H. E.; Toppare, L. *Sensors Actuators, B Chem.* **2016**, *228*, 278–286.
- (7) Li, W.; Guo, Y.; Shi, J.; Yu, H.; Meng, H. *Macromolecules* **2016**, *49* (19), 7211–7219.
- (8) Dai, L. In *Intelligent Macromolecules for Smart Devices: From Materials Synthesis to Device Applications*; Springer, 2004.
- (9) Cheng, Y.-J.; Yang, S.-H.; Hsu, C.-S. *Chem. Rev. (Washington, DC, U. S.)* **2009**, *109* (11), 5868–5923.
- (10) Tress, W. *Organic Solar Cells*; Springer, 2014.
- (11) Molapo, K. M.; Ntangili, P. M.; Ajayi, R. F.; Mbambisa, G.; Mailu, S. M.;

- Njomo, N.; Masikini, M.; Baker, P.; Iwuoha, E. I. *Int. J. Electrochem. Sci.* **2012**, *7* (12), 11859–11875.
- (12) Bredas, J. L.; Street, G. B. *Acc. Chem. Res.*, **1985**, *18* (10), 309–315.
- (13) Kar, P. *Doping in Conjugated Polymers*; Wiley, 2013.
- (14) Radhakrishnan, S.; Ananthakrishnan, S. J.; Somanathan, N. *Bull. Mater. Sci.* **2011**, *34* (4), 713–726.
- (15) Cheng, Y.-J.; Yang, S.-H.; Hsu, C.-S. *Chem. Rev.* **2009**, *109* (11), 5868–5923.
- (16) DelZoppo, M.; Castiglioni, C.; Gerola, V.; Zuliani, P.; Zerbi, G. *J. Opt. Soc. Am. B* **1998**, *15* (1), 308–317.
- (17) Roncali, J. *Macromol. Rapid Commun.* **2007**, *28* (17), 1761–1775.
- (18) Hess, A. B.; Schaad L. J. *Am. Chem. Soc.* **1973**, *95* (12), 3907–3912.
- (19) Bundgaard, E.; Krebs, F. C. *Sol. Energy Mater. Sol. Cells* **2007**, *91* (11), 954–985.
- (20) Gao, Y. L.; Liu, J.; Huang, D. H. *Synth. Met.* **2009**, *159* (14), 1450–1453.
- (21) Nalwa, S. H. *Handbook of Advanced Electronic and Photonic Materials and Devices*; Academic Press, 2001.
- (22) Xu, T.; Yu, L. *Mater. Today* **2014**, *17* (1), 11–15.
- (23) Kroon, R.; Lenes, M.; Hummelen, J. C.; Blom, P. W. M.; de Boer, B. *Polymer Reviews* **2008**, *48*, 531–582.
- (24) Roncali, J. *Chem. Rev.* **1997**, *97* (1), 173–206.
- (25) Havinga, E. E.; Hoeve, W.; Wynberg, H. *Synth. Met.* **1993**, *55* (1), 299–306.
- (26) Naik, M. a; Raghavendra, M.; Bhaskar, R.; Siram, K.; Patil, S. *Materials (Basel)*. 1115–1123.

- (27) Song, H. J.; Lee, J. Y.; Lee, E. J.; Moon, D. K. *Eur. Polym. J.* **2013**, 49 (10), 3261-3270.
- (28) Pourjafari, D.; Vazquez, A.; Cavazos, J.; Gomez, I. *Soft Mater.* **2014**, 12 (4), 380–386.
- (29) Feldberg, S. W.; Jeftic, L. *J. Phys. Chem.* **1972**, 76 (17), 2439–2446.
- (30) Carothers, W. H. *J. Am. Chem. Soc.* **1929**, 51 (8), 2548–2559.
- (31) Abu-Thabit, N. Y. *J. Chem. Educ.* **2016**, 93 (9), 1606–1611.
- (32) Negishi, S. X. and E. H. K. and A. W. and E. *Sci. Technol. Adv. Mater.* **2014**, 15 (4), 44201.
- (33) Bäckvall, J.-E. *Sci. Backgr. Nobel Prize Chem.* **2010**, 50005, 1–12.
- (34) Kim, J. Y.; Yang, C.; Yeom, H. R.; Kim, Y. *Energy Environ. Sci.* **2013**, 6 (6), 1909–1916.
- (35) Chang, D. W.; Ko, S. J.; Kim, J. Y.; Dai, L.; Baek, J. B. *Synth. Met.* **2012**, 162 (13), 1169–1176.
- (36) Dutta, G. K.; Patil, S. *Org. Electron.* **2012**, 13 (7), 1266–1276.
- (37) Balan, A.; Gunbas, G.; Durmus, A.; Toppare, L. *Chem. Mater.* **2008**, 20, 7510-7513.
- (38) Baran, D.; Balan, A.; Celebi, S.; Meana Esteban, B.; Neugebauer, H.; Sariciftci, N. S.; Toppare, L. *Chem. Mater.* **2010**, 22 (9), 2978–2987.
- (39) Unay, H.; Unlu, N. A.; Hizalan, G.; Hacioglu, S. O.; Yildiz, D. E.; Toppare, L.; Cirpan, A. *J. Polym. Sci. Part A Polym. Chem.* **2014**, 53 (4), 528–535.
- (40) Erlik, O.; Unlu, N. A.; Hizalan, G.; Hacioglu, S. O.; Comez, S.; Yildiz, E. D.; Toppare, L.; Cirpan, A. *J. Polym. Sci. Part A Polym. Chem.* **2015**, 53 (13), 1541–1547.

- (41) Zhang, Z.; Peng, B.; Liu, B.; Pan, C.; Li, Y.; He, Y.; Zhou, K.; Zou, Y. *Polym. Chem.* **2010**, *1* (9), 1441.
- (42) Liao, Y.; Hu, J.; Xie, Q.; Peng, D.; Liu, Y.; Zhu, C.; Zhong, C. *Spectrochim. Acta - Part A Mol. Biomol. Spectrosc.* **2016**, *153*, 681–687.
- (43) Imai, K.; Kihara, Y.; Kimoto, A.; Abe, J.; Tamai, Y.; Nemoto, N. *Polym. J.* **2011**, *43* (1), 58–65.
- (44) Kim, H. G.; Jo, S. B.; Shim, C.; Lee, J.; Shin, J.; Cho, E. C.; Ihn, S.-G.; Choi, Y. S.; Kim, Y.; Cho, K. *J. Mater. Chem.* **2012**, *22* (34), 17709.
- (45) Gao, C.; Wang, L.; Wang, H. *Polym. Chem.* **2014**, *5*, 5200–5210.
- (46) Scrosati, B. *Mater. Sci. Forum* **1989**, *42* (December), 207–220.
- (47) Snook, G. A.; Kao, P.; Best, A. S. *J. Power Sources* **2010**, *196*, 1–12.
- (48) Xu, C.; Liu, L.; Legenski, S. E.; Ning, D.; Taya, M. *J. Mater. Res.* **2011**, *19* (7), 2072–2080.
- (49) Rosseinsky, D. R.; Mortimer, R. J. *Adv. Mater.* **2001**, *13* (11), 783–793.
- (50) Ebisawa, F.; Kurokawa, T.; Nara, S. *J. Appl. Phys.* **1983**, *54* (6), 3255–3259.
- (51) White, M. S.; Kaltenbrunner, M.; Głowacki, E. D.; Gutnichenko, K.; Kettlgruber, G.; Graz, I.; Aazou, S.; Ulbricht, C.; Egbe, D. a. M.; Miron, M. C.; Major, Z.; Scharber, M. C.; Sekitani, T.; Someya, T.; Bauer, S.; Sariciftci, N. S. *Nat. Photonics* **2013**, *7* (10), 811–816.
- (52) Azeri, O.; Aktas E.; Halls, Istanbuloglu C.; Hacıoglu, S. O.; Cevher, S. C.; Toppare, L.; Cirpan, *Polymer* **2017**, *133*, 60-67.
- (53) Suhag, N.; Singh, S. *Int. J. Enhanc. Res. Sci. Technol. Eng.* **2015**, *4* (8), 28–36.
- (54) Deb, S. K. *Appl. Opt.* **1969**, *8*, 192-195.

- (55) Trong, L. D.; Dinh, N. N.; Thanh, D. H. *Mater. Sci. Appl.* **2016**, 7 (11), 702–709.
- (56) Quang L. N.; Ashrit, P.; Girouard, F. E.; Truong V. *SPIE Proceedings* **1991**, 1401,11.
- (57) Kanbara, T.; Yamamoto, T. *Macromolecules* **1993**, 26, 1975–1979.
- (58) Bird, C. L.; Kuhn, a. T. *Chem. Soc. Rev.* **1981**, 10 (1), 49.
- (59) Mortimer, R. J.; Rosseinsky, D. R.; Monk, P. M. S. *Electrochromic Mater. Devices* **2015**, 77, 1–638.
- (60) Yağmur, İ.; Ak, M.; Bayrakçeken, A. *Smart Mater. Struct.* **2013**, 22 (11), 115022.
- (61) Babudri, F.; Farinola, G. M.; Naso, F.; Ragni, R. *Chem. Commun.* **2007**, No. 10, 1003–1022.
- (62) Argun, A. A.; Aubert, P. H.; Thompson, B. C.; Schwendeman, I.; Gaupp, C. L.; Hwang, J.; Pinto, N. J.; Tanner, D. B.; MacDiarmid, A. G.; Reynolds, J. R. *Chem. Mater.* **2004**, 16 (23), 4401–4412.
- (63) Monk, P.; Mortimer, R.; Rosseinsky, D. *Electrochromism and Electrochromic Devices*; Cambridge, 2007.
- (64) Mohammad Bagher, A. *Int. J. Renew. Sustain. Energy* **2014**, 3 (3), 53.
- (65) Tang, C. W. *Appl. Phys. Lett.* **1986**, 48 (2), 183–185.
- (66) Fung, D. D. S.; Choy, W. C. H. In *Control*; Choy, W. C. H. *Introduction to Organic Solar Cells*, Springer, 2013.
- (67) Hiramoto, M.; Suezaki, M.; Yokoyama, M. *Chem. Lett.* **1990**, 327–330.
- (68) Ameri, T.; Dennler, G.; Lungenschmied, C.; Brabec, C. J. *Energy Environ. Sci.* **2009**, 2 (4), 347–363.

- (69) Yu, G.; Heeger, A. J. *J. Appl. Phys.* **1995**, *78* (7), 4510–4515.
- (70) Huang, H.; Deng, W. *Organic and Hybrid Solar Cells*, Springer, 2014.
- (71) Scharber, M. C.; Sariciftci, N. S. *Prog. Polym. Sci.* **2013**, *38* (12), 1929–1940.
- (72) Vivek, K. a; Agrawal, G. D. *Int. J. Res. Eng. Technol.* **2014**, *3* (9), 2319–2322.
- (73) Abdulrazzaq, O. a.; Saini, V.; Bourdo, S.; Dervishi, E.; Biris, A. S. *Part. Sci. Technol.* **2013**, *31* (5), 427–442.
- (74) Gunes, S.; Neugebauer, H.; Sariciftci, N. S. *Chem. Rev.* **2007**, *107*, 1324–1338.
- (75) Elumalai, N. K.; Uddin, A. *Energy Environ. Sci.* **2016**, *9* (2), 391–410.
- (76) Scharber, M. C.; Mühlbacher, D.; Koppe, M.; Denk, P.; Waldauf, C.; Heeger, A. J.; Brabec, C. J. *Adv. Mater.* **2006**, *18* (6), 789–794.
- (77) Barry P. Rand, H. R. *Organic Solar Cells: Fundamentals, Devices, and Upscaling*, CRC Press, 2014.
- (78) Benanti, T. L.; Venkataraman, D. *Photosynth. Res.* **2006**, *87* (1), 73–81.
- (79) Boyuan Qi and Jizheng Wang. *Sol. Energy Mater. Sol. Cells* **2010**, *94* (8), 1309–1313.
- (80) Jao, M.-H.; Liao, H.-C.; Su, W.-F. *J. Mater. Chem. A* **2016**, *0*, 1–18.
- (81) Keshtov, M. L.; Marochkin, D. V.; Kochurov, V. S.; Khokhlov, A. R.; Koukaras, E. N.; Sharma, G. D. *Polym. Chem.* **2013**, *4* (14), 4033.
- (82) Kim, M.-J.; Kim, J.-H.; Ahn, J. J.; Hwang, D.-H. *Dye. Pigment.* **2016**, *133*, 324–332.
- (83) Marin, L.; Lutsen, L.; Vanderzande, D.; Maes, W. *Org. Biomol. Chem.* **2013**, *11* (35), 5866–5876.

- (84) Caffy, F.; Delbosc, N.; Chávez, P.; Lévêque, P.; Faure-Vincent, J.; Travers, J.-P.; Djurado, D.; Pécaut, J.; Grévin, B.; Lemaitre, N.; Leclerc, N.; Demadrille, R. *Polym. Chem.* **2016**, *7* (25), 4129-4286.
- (85) Lee, Y.; Nam, Y. M.; Jo, W. H. *J. Mater. Chem.* **2011**, *21* (24), 8583–8590.
- (86) Tessarolo, M.; Gedefaw, D.; Bolognesi, M.; Liscio, F.; Henriksson, P.; Zhuang, W.; Milita, S.; Muccini, M.; Wang, E.; Seri, M.; Andersson, M. R. *J. Mater. Chem. A* **2014**, *2*, 11162-11170.
- (87) Wang, E.; Hou, L.; Wang, Z.; Ma, Z.; Hellström, S.; Zhuang, W.; Zhang, F.; Inganäs, O.; Andersson, M. R. *Macromolecules* **2011**, *44* (7), 2067–2073.
- (88) Kitazawa, D.; Watanabe, N.; Yamamoto, S.; Tsukamoto, J. *Sol. Energy Mater. Sol. Cells* **2012**, *98*, 203–207.
- (89) Liu, D.; Zhao, W.; Zhang, S.; Ye, L.; Zheng, Z.; Cui, Y.; Chen, Y.; Hou, J. *Macromolecules* **2015**, *48* (15), 5172–5178.
- (90) Chen, H.-C.; Chen, Y.-H.; Liu, C.-H.; Hsu, Y.-H.; Chien, Y.-C.; Chuang, W.-T.; Cheng, C.-Y.; Liu, C.-L.; Chou, S.-W.; Tung, S.-H.; Chou, P.-T. *Polym. Chem.* **2013**, *4* (11), 3411–3418.
- (91) Hou, J.; Park, M.; Zhang, S.; Yao, Y.; Chen, L.-M.; Li, J.-H.; Yang, Y. *Macromolecules* **2008**, *41* (16), 6012–6018.
- (92) Kim, J. H.; Song, C. E.; Kim, H. U.; Kang, I. N.; Shin, W. S.; Park, M. J.; Hwang, D. H. *J. Polym. Sci. Part A Polym. Chem.* **2015**, *53*, 1904-1914. .
- (93) Gao, Z.; Qu, B.; Wu, H.; Gao, C.; Yang, H.; Zhang, L.; Xiao, L.; Chen, Z.; Gong, Q. *J. Appl. Polym. Sci.* **2014**, *131* (10), 40279-40288.
- (94) Balan, A.; Baran, D.; Toppare, L. *Polym. Chem.* **2011**, *2* (5), 1029.
- (95) Dong, Y.; Cai, W. Z.; Hu, X. W.; Zhong, C. M.; Huang, F.; Cao, Y. *Polymer (Guildf)*. **2012**, *53* (7), 1465–1472.

- (96) Zhang, L.; He, C.; Chen, J.; Yuan, P.; Huang, L.; Zhang, C.; Cai, W.; Liu, Z.; Cao, Y. *Macromolecules* **2010**, *43* (23), 9771–9778.
- (97) Cevher, S. C.; Hizalan, G.; Temiz, C.; Udum, Y. A.; Toppare, L.; Cirpan, A. *Polym. (United Kingdom)* **2016**, *101*, 208–216.
- (98) Fu, Y.; Cha, H.; Song, S.; Lee, G.-Y.; Eon Park, C.; Park, T. *J. Polym. Sci. Part A Polym. Chem.* **2013**, *51* (2), 372–382.
- (99) Wang, K.; Zhang, Z. G.; Fu, Q.; Li, Y. *Macromol. Chem. Phys.* **2014**, *215* (7), 597–603.
- (100) Kim, J. H.; Kim, H. U.; Lee, J. K.; Park, M. J.; Hyun, M. H.; Hwang, D. H. *Synth. Met.* **2013**, *179*, 18–26.
- (101) Kim, J. H.; Kim, H. U.; Song, C. E.; Kang, I. N.; Lee, J. K.; Shin, W. S.; Hwang, D. H. *Sol. Energy Mater. Sol. Cells* **2013**, *108*, 113–125.
- (102) Wang, X. C.; Sun, Y. P.; Chen, S.; Guo, X.; Zhang, M. J.; Li, X. Y.; Li, Y. F.; Wang, H. Q. *Macromolecules* **2012**, *45*, 1208–1216.
- (103) Lei, T. *Design, Synthesis, and Structure-Property Relationship Study of Polymer Field-Effect Transistors*; Springer, 2015.
- (104) Hizalan, G.; Balan, A.; Baran, D.; Toppare, L. *J. Mater. Chem.* **2011**, *21* (6), 1804-1809.
- (105) Lei, T. *Design, Synthesis, and Structure-Property Relationship Study of Polymer Field-Effect Transistors*; Springer, 2015.
- (106) Wöhrle, D.; Meissner, D. *Adv. Mater.* **1991**, *3* (3), 129–138.
- (107) Chen, H.-Y.; Hou, J.; Zhang, S.; Liang, Y.; Yang, G.; Yang, Y.; Yu, L.; Wu, Y.; Li, G. *Nat. Photon.* **2009**, *3*, 649-653.
- (108) Kleinhenz, N.; Yang, L.; Zhou, H.; Price, S. C.; You, W. *Macromolecules* **2011**, *44* (4), 872–877.

- (109) Ouyang, D.; Xiao, M.; Zhu, D.; Zhu, W.; Du, Z.; Wang, N.; Zhou, Y.; Bao, X.; Yang, R. *Polym. Chem.* **2015**, *6* (1), 55–63.
- (110) Kim, J. H.; Song, C. E.; Kim, H. U.; Kang, I. N.; Shin, W. S.; Park, M. J.; Hwang, D. H. *J. Polym. Sci. Part A Polym. Chem.* **2013**, *51* (19), 4136–4149.
- (111) Liu, C.; Wang, K.; Hu, X.; Yang, Y.; Hsu, C.; Zhang, W.; Xiao, S.; Gong, X.; Cao, Y. *ACS Appl. Mater. Interfaces* **2013**, *5*, 12163–12167.
- (112) Zhang, K.; Hu, Z.; Duan, C.; Ying, L.; Huang, F. *Macromolecules*, **2010**, *43*, 9771–9778.

APPENDICES

A. NMR DATA

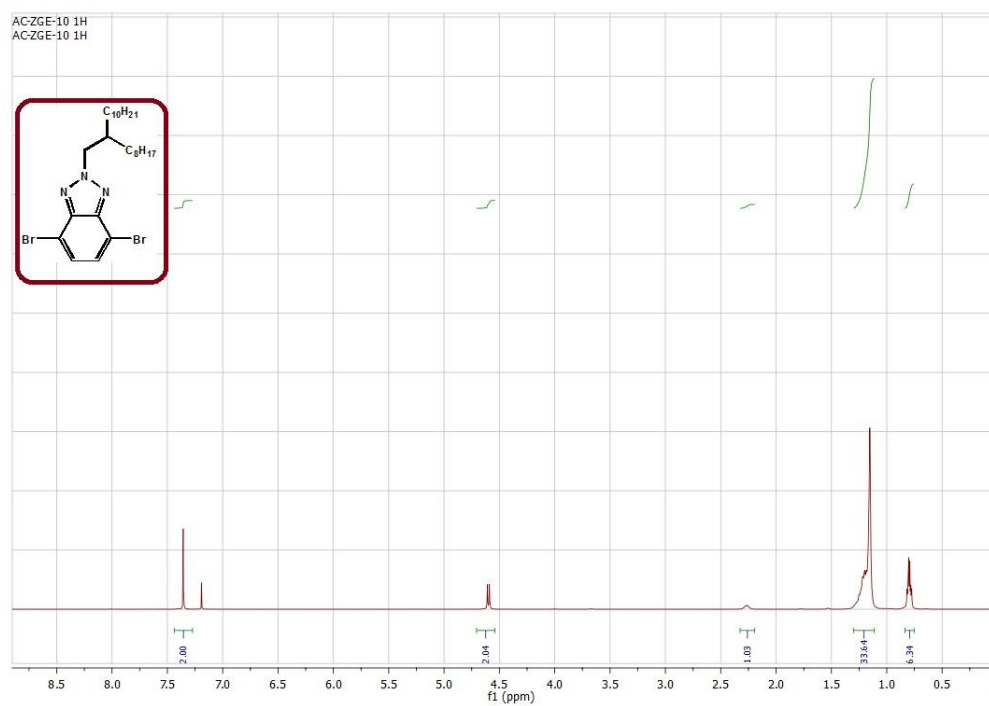


Figure 38. ¹H NMR result of 4,7-dibromo-2-(2-octyldodecyl)-2H-benzo[d][1,2,3]triazole

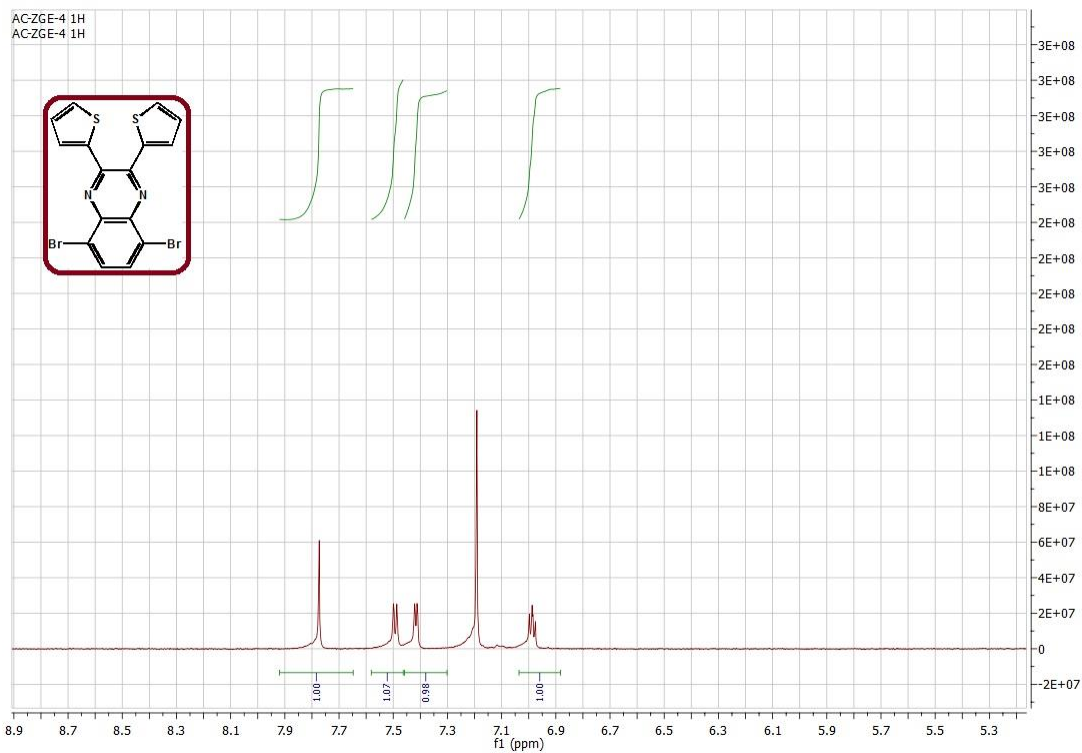


Figure 39. ^1H NMR result of 5,8-dibromo-2,3-di(thiophen-2-yl)quinoxaline

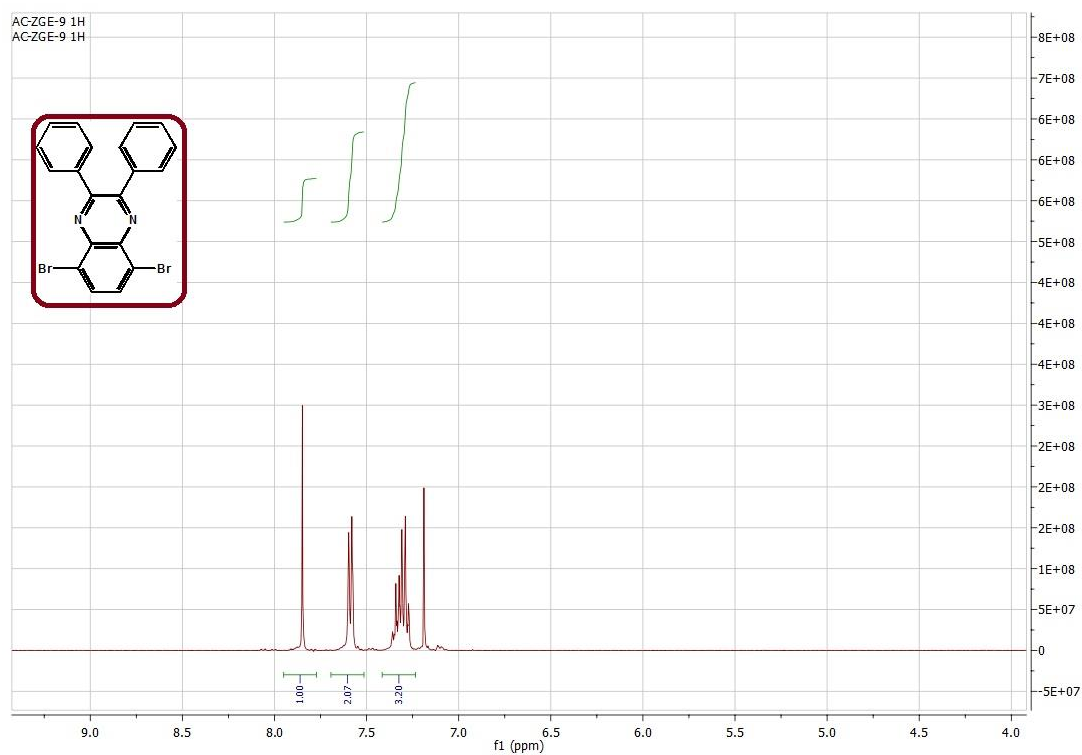
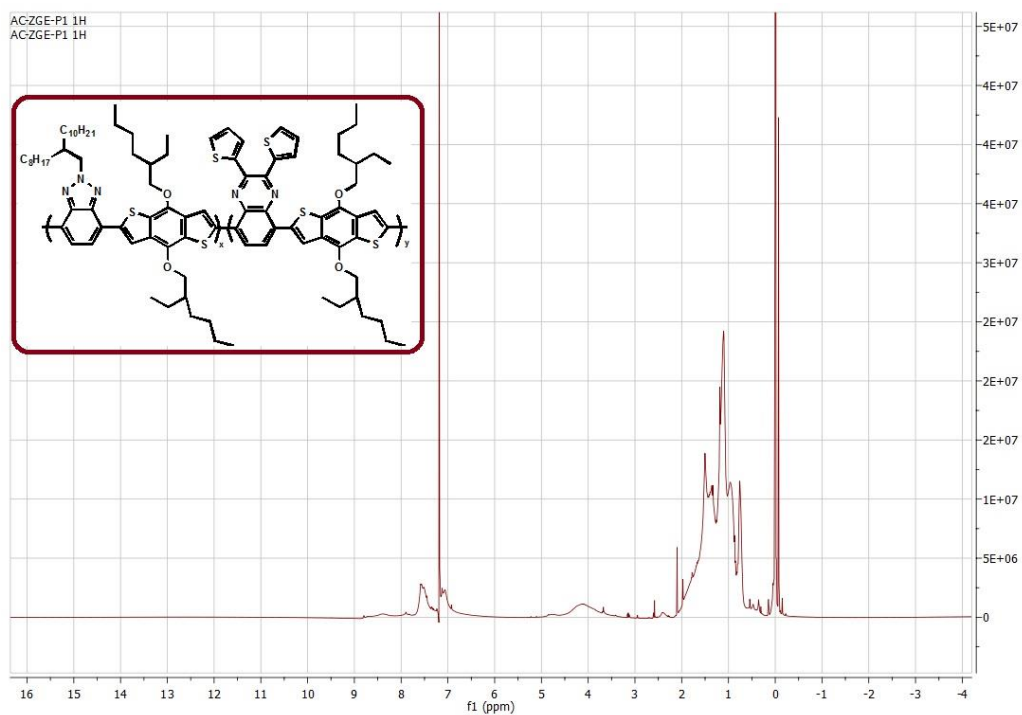
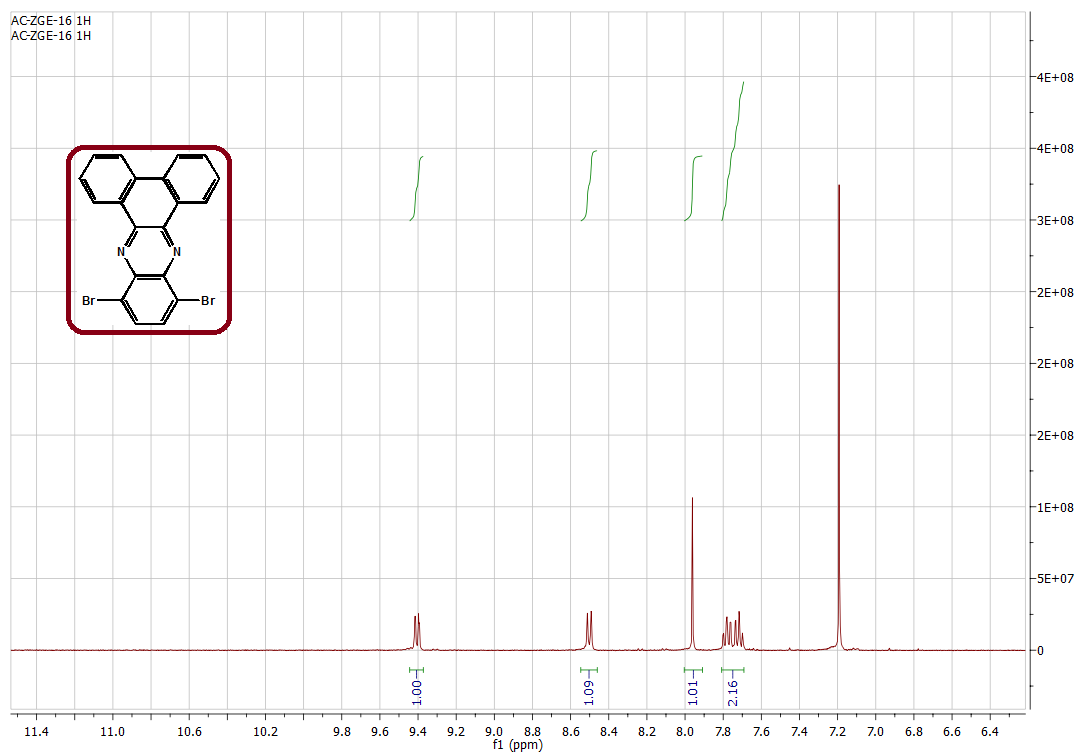
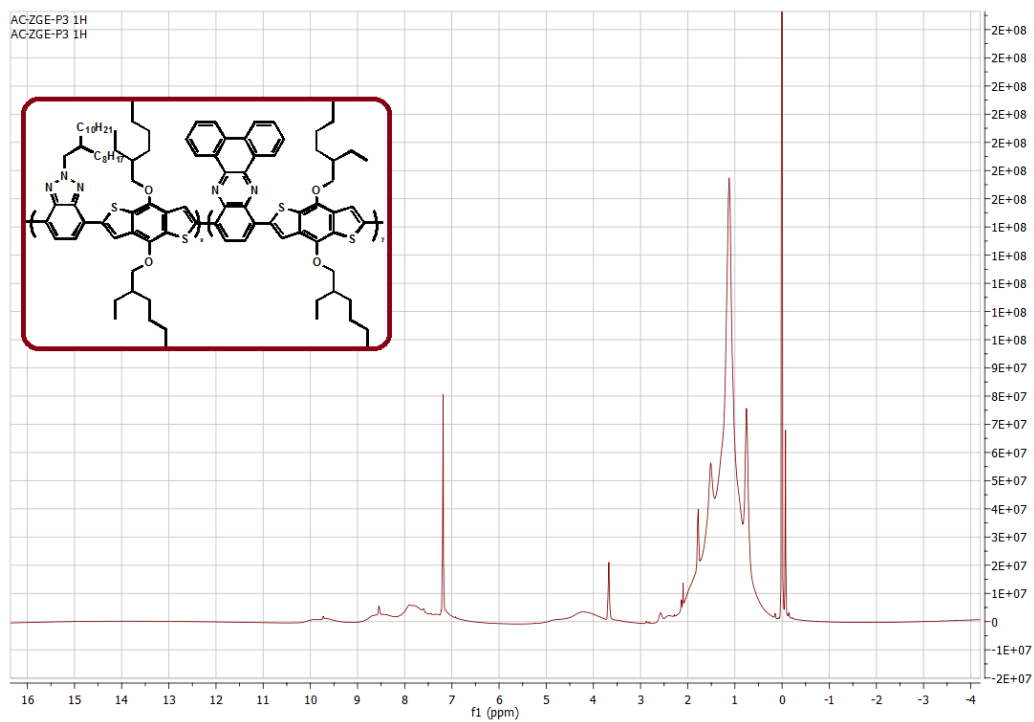
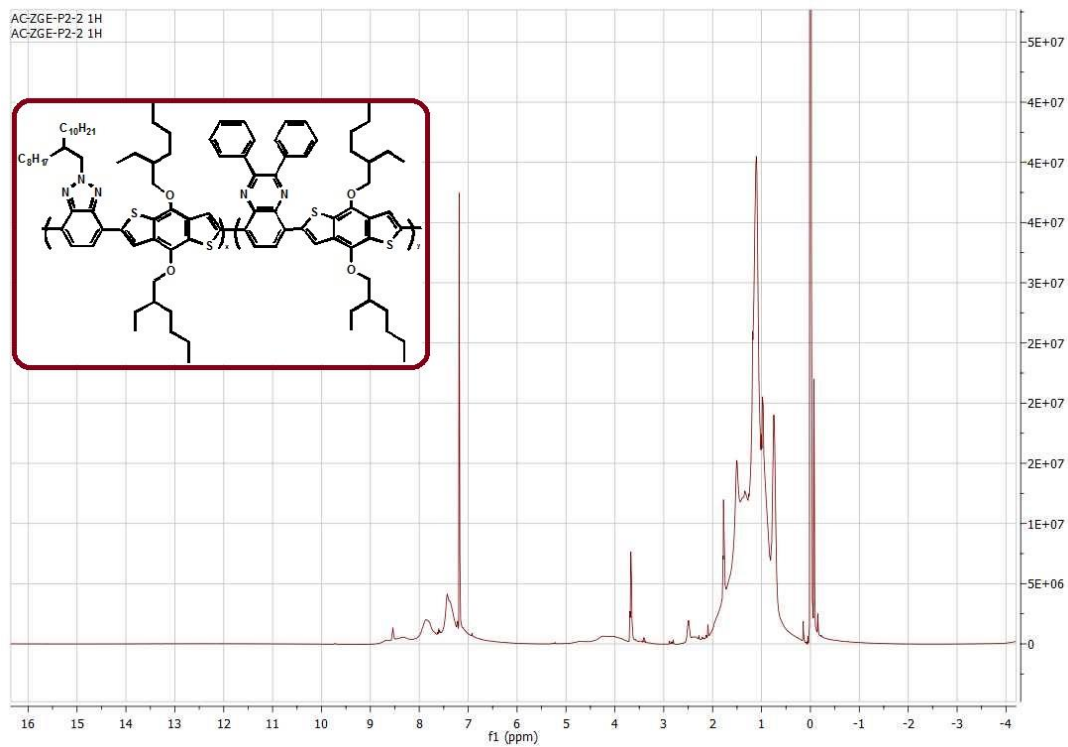


Figure 40. ^1H NMR result of 5,8-dibromo-2,3-diphenylquinoxaline





B. THERMAL ANALYSES RESULTS

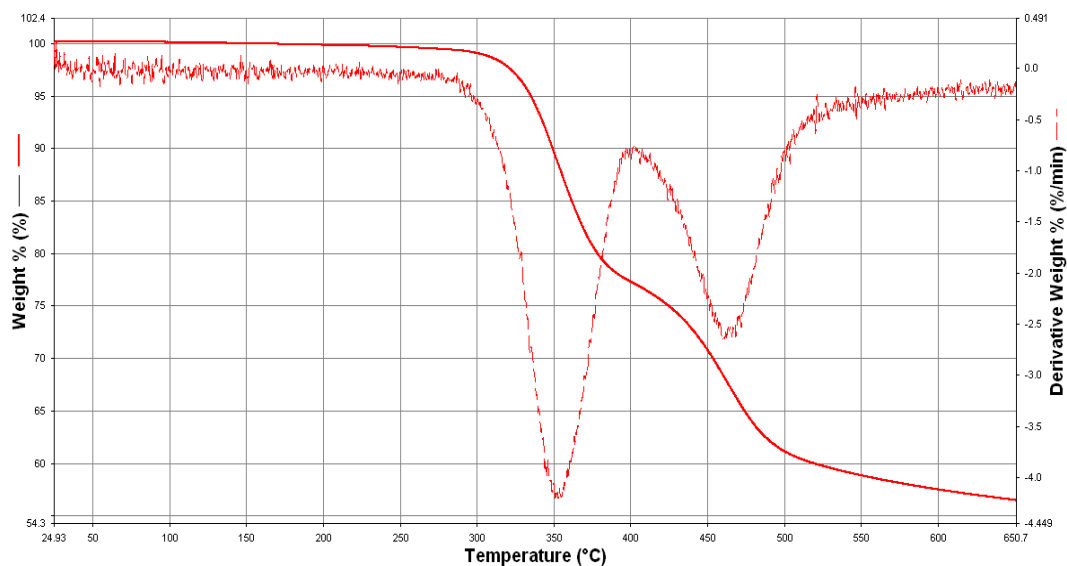


Figure 45. TGA result of P1

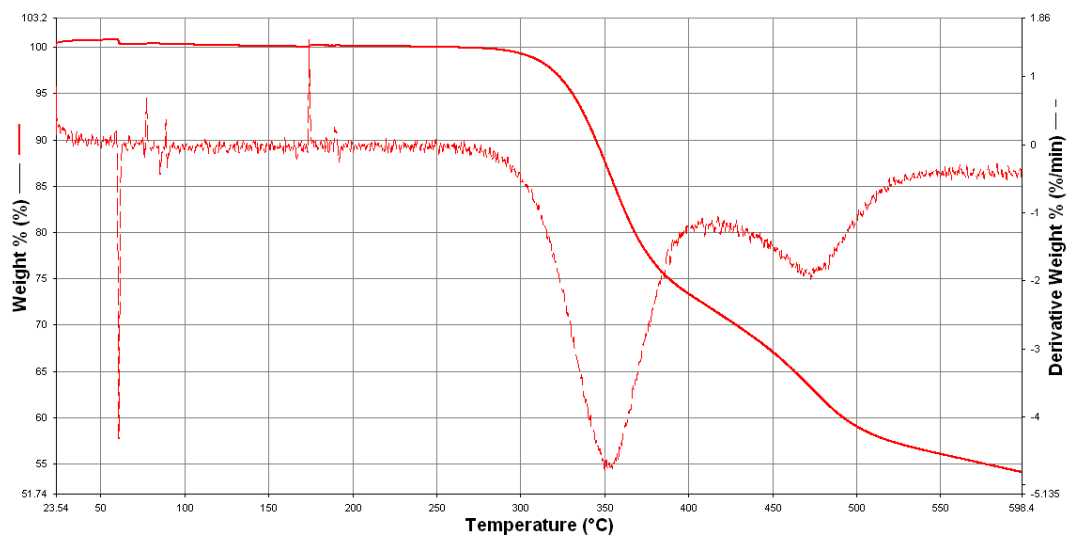


Figure 46. TGA result of P2

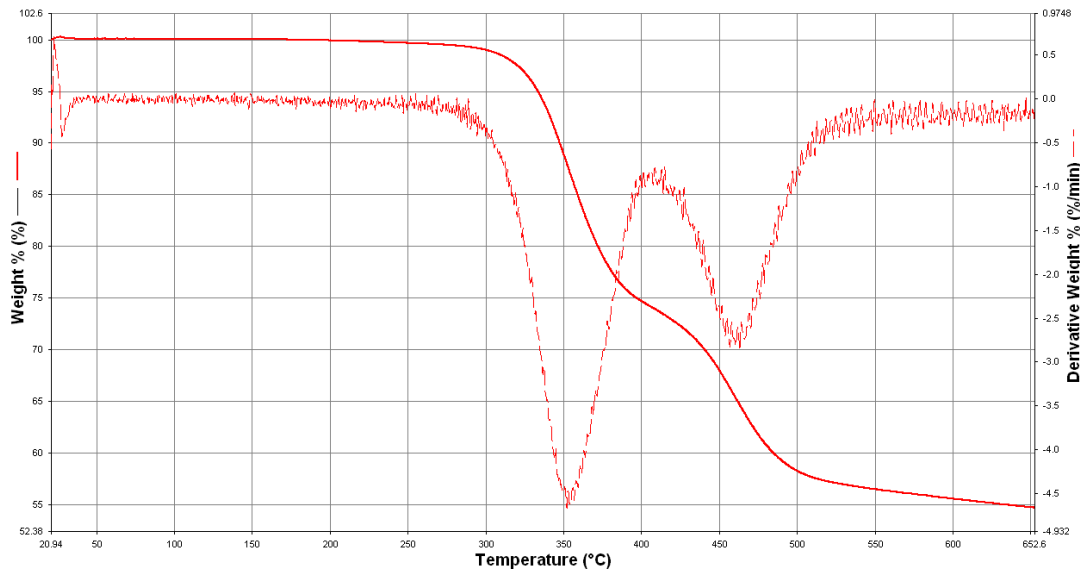


Figure 47.TGA result of P3

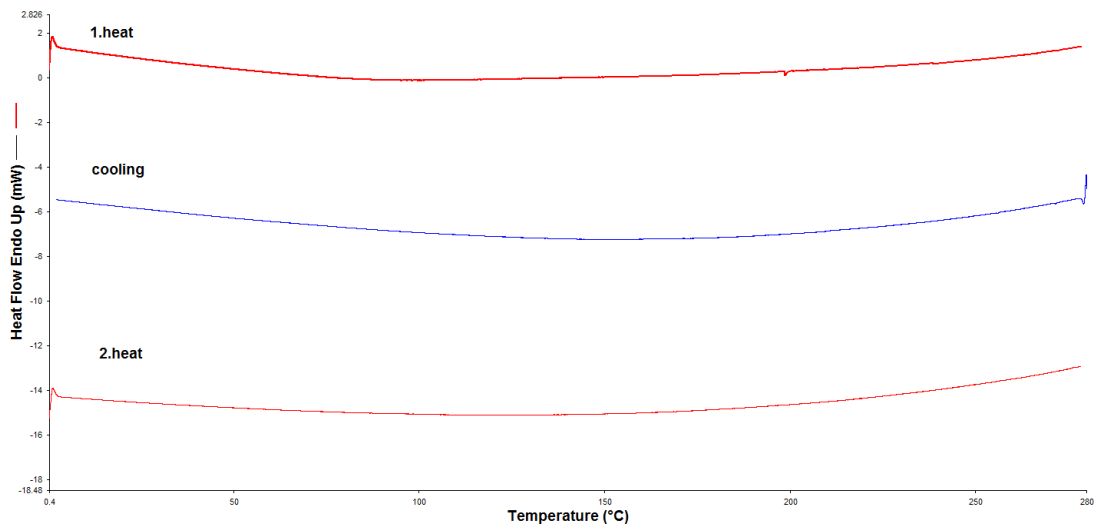


Figure 48. DSC result of P1

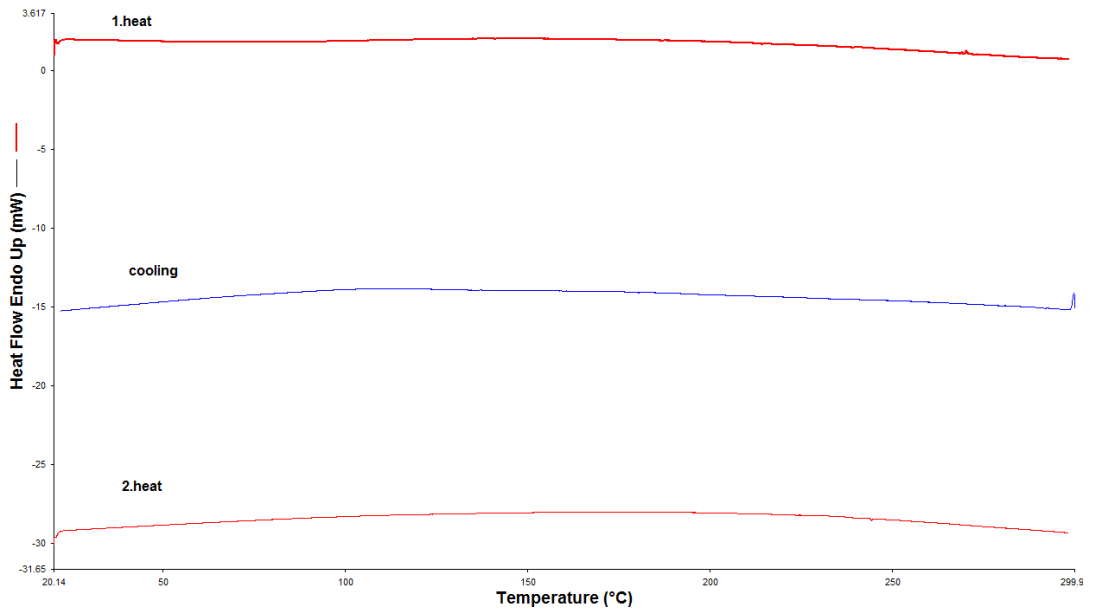


Figure 49. DSC result of P2

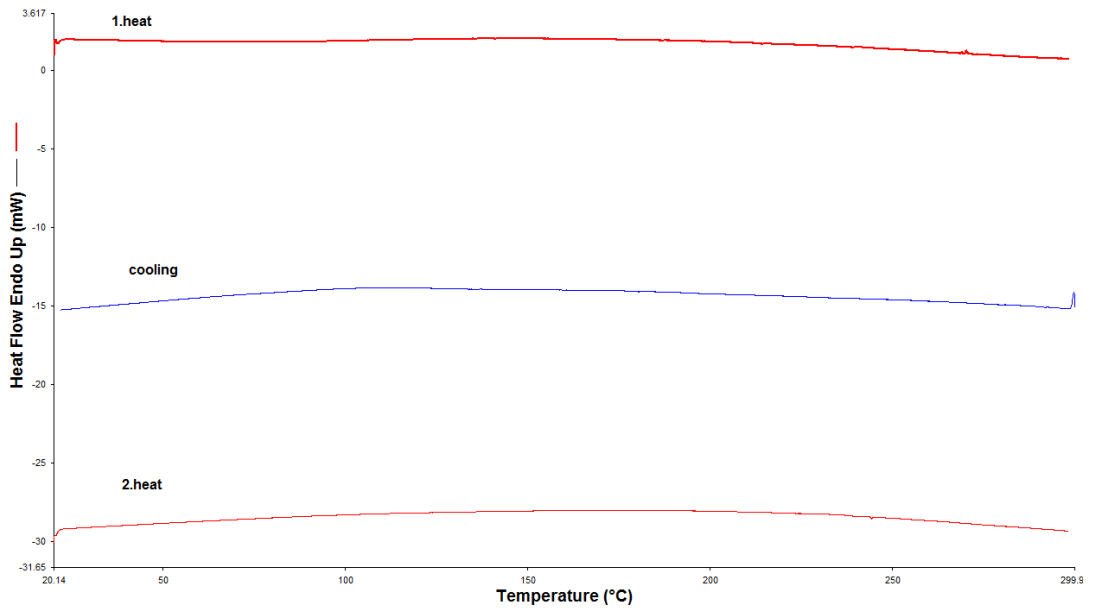


Figure 50. DSC result of P3